ANNUAL REVIEWS

Annual Review of Nuclear and Particle Science

Recent Progress in the Physics of Axions and Axion-Like Particles

Kiwoon Choi, Sang Hui Im, and Chang Sub Shin

Center for Theoretical Physics of the Universe, Institute for Basic Science, Daejeon 34126, South Korea; email: kchoi@ibs.re.kr

Annu. Rev. Nucl. Part. Sci. 2021. 71:225–52

First published as a Review in Advance on June 17, 2021

The *Annual Review of Nuclear and Particle Science* is online at nucl.annualreviews.org

https://doi.org/10.1146/annurev-nucl-120720-031147

Keywords

axions, axion-like particles, axion couplings, axion scales, axion cosmology, axion detection, axion landscape

Abstract

The axion is a light pseudoscalar particle postulated to solve issues with the Standard Model, including the strong CP problem and the origin of dark matter. In recent years, there has been remarkable progress in the physics of axions in several directions. An unusual type of axion-like particle termed the relaxion was proposed as a new solution to the weak scale hierarchy problem. There are also new ideas for laboratory, astrophysical, or cosmological searches for axions; such searches can probe a wide range of model parameters that were previously inaccessible. On the formal theory side, the weak gravity conjecture indicates a tension between quantum gravity and a trans-Planckian axion field excursion. Many of these developments involve axions with hierarchical couplings. In this article, we review recent progress in axion physics, with particular attention paid to hierarchies between axion couplings. We emphasize that the parameter regions of hierarchical axion couplings are the most accessible experimentally. Moreover, such regions are often where important theoretical questions in the field are addressed, and they can result from simple model-building mechanisms.

Contents

1. INTRODUCTION

Axions and axion-like particles (ALPs) are among the most compelling candidates for physics beyond the Standard Model (SM) of particle physics (1–3). They often have good physics motivations and naturally arise in fundamental theories such as string theory (4, 5). In some cases, an axion refers to a specific type of pseudo-Nambu-Goldstone boson designed to solve the strong CP problem (6–8). In this article, we refer to such an axion as a quantum chromodynamics (QCD) axion and use the term axions (and sometimes the term ALPs) for generic pseudo-Nambu-Goldstone bosons associated with nonlinearly realized approximate global $U(1)$ symmetries.

Many different types of axions have been discussed in particle physics and cosmology. Some of them are introduced to solve so-called naturalness problems. The best-known example is a QCD axion that solves the strong CP problem (6–8). Another example is an axion for cosmic inflation (9), which would solve the naturalness problems of Big Bang cosmology while avoiding unnatural fine-tuning in the underlying UV theory. An unusual type of ALP termed the relaxion was recently proposed as a new solution to the weak scale hierarchy problem (10). Light axions, regardless of their role in naturalness problems, are a compelling candidate for the dark matter (DM) in our Universe (11–14). Although the data are not convincing enough, a few astrophysical anomalies might be explained by axions with certain specific masses and coupling (15–17).

In recent years, there has been significant progress in several directions in the physics of axions. Such developments include the relaxion solution to the weak scale hierarchy problem (10), which has a variety of interesting phenomenological implications (18–20). New ideas for axion searches in laboratory experiments have been proposed (21–23), and such searches can probe a wide range of axion masses and couplings that were not accessible before. There are also studies on the gravitational probe of ultralight axion DM (24), as well as axion superradiance from black holes (BHs) (5). In addition, new theory concepts have generated both constraints and model-building ideas. On one hand, it is argued that quantum gravity provides a nontrivial lower bound on axion couplings (25), which might be in conflict with the requirement in some models of inflation for trans-Planckian axion field excursions (26–30). On the other hand, mechanisms have been presented to naturally produce large hierarchies in axion couplings (31–38).

Many of these developments suggest that the landscape of axion models is much broader than commonly realized. Of particular interest are regions where axion couplings have large hierarchies. As discussed below in more detail, those regions are generally the most accessible experimentally,

and they are often where important theoretical questions in the field are addressed. In actuality, large hierarchies among axion couplings are not unexpected. They are technically natural and can result from simple model-building mechanisms.

This article is organized as follows. In Section 2, we introduce the relevant axion couplings and scale parameters and present the observational constraints on those parameters, including the projected sensitivity limits of the planned experiments. In Section 3, we present some examples of well-motivated axion coupling hierarchies and discuss model-building attempts to generate those hierarchies in low-energy effective theory. We conclude and summarize in Section 4.

2. AXION COUPLINGS AND SCALES

Axions are periodic scalar fields and characterized by a scale f_a termed the axion decay constant, which defines the full field range of the canonically normalized axion:

$$a \cong a + 2\pi f_a. \tag{1.}$$

Such axions may originate from the phase of complex scalar field (39–42) as

$$\sigma = \rho e^{ia/f_a} \quad (f_a = \sqrt{2}\langle\rho\rangle), \tag{2.}$$

or the zero mode of a p-form gauge field $A^{(p)}$ in models with extra dimension such as compactified string theories[1] (4, 43–45):

$$A^{(p)}_{[m_1 m_2 .. m_p]}(x,y) = a(x)\omega^{(p)}_{[m_1 m_2 .. m_p]}(y), \tag{3.}$$

where x^μ and y^m are the coordinates of four-dimensional Minkowski spacetime and the compact internal space Y, respectively, and $\omega^{(p)}$ is a harmonic p-form in Y. In the latter case, axion periodicity is assured by Dirac quantization of the axionic string, which is a low-energy remnant of the brane that couples (electrically or magnetically) to $A^{(p)}$ in the underlying UV theory. In that description, the gauge equivalence of $A^{(p)}$ on a p-cycle in Y, which determines the value of f_a, is fixed by the couplings and scales involved in compactification (4, 45, 46).

Axions, regardless of their UV origin, can be naturally light if the theory admits an approximate $U(1)$ symmetry realized as a shift of the axion field:

$$U(1)_{\rm PQ} \ : \ a(x) \to a(x) + \text{constant}. \tag{4.}$$

This is termed Peccei-Quinn (PQ) symmetry. For $a(x)$ originating from the phase of a complex scalar field, $U(1)_{\rm PQ}$ may arise as an accidental symmetry of the low-energy effective theory. For $a(x)$ from a p-form gauge field, it is the low-energy remnant of the p-form gauge symmetry $A^{(p)} \to A^{(p)} + {\rm d}C^{(p-1)}$ in the underlying higher-dimensional theory.

A key parameter for axion physics is PQ-breaking coupling $g_{a\Lambda}$ that generates the leading a-dependent terms in the axion potential. The corresponding potential can often be approximated by a sinusoidal function:

$$V(a) \simeq -\Lambda^4 \cos(g_{a\Lambda} a). \tag{5.}$$

[1] For $p \geq 2$, there can be additional axions originating from the component $A^{(p)}_{[\mu\nu m_1 .. m_{p-2}]}$.

This can also be written as

$$V(a) \simeq -\Lambda^4 \cos\left(N_{\rm DW}\frac{a}{f_a}\right), \tag{6.}$$

where $N_{\rm DW}$ is the number of (approximately) degenerate vacua found over the full field range $2\pi f_a$, which is termed the domain wall number. The coupling $g_{a\Lambda} = N_{\rm DW}/f_a$ also defines the field range over which the axion potential is monotonically changing:

$$\Delta a \equiv \frac{\pi}{g_{a\Lambda}} = \pi\frac{f_a}{N_{\rm DW}}, \tag{7.}$$

which may set an upper bound on the possible cosmological excursion of the axion field.

2.1. Axions in Cosmology

Axions can play many important roles in cosmology (2). Here we present three examples that are relevant for our later discussion of axion coupling hierarchies.

2.1.1. Axion inflation. An axion field with trans-Planckian $f_a/N_{\rm DW} > M_P \simeq 2.4 \times 10^{18}$ GeV can play the role of an inflaton in the model of natural inflation (9). For the inflation potential given by Equation 6, one finds

$$\epsilon \sim \eta \sim \frac{1}{N_e} \sim \left(\frac{M_P}{f_a/N_{\rm DW}}\right)^2, \tag{8.}$$

where $\epsilon = M_P^2(\partial_a V/V)^2/2$ and $\eta = M_P^2(\partial_a^2 V/V)$ are the slow roll parameters and N_e is the number of e-foldings. Then the observed cosmic microwave background (CMB) power spectrum implies $m_a \sim \mathcal{H}_{\rm inf}/\sqrt{N_e} \sim 10^{13}$ GeV, where $\mathcal{H}_{\rm inf} \sim \Lambda^2/M_P$ is the inflationary Hubble scale (9, 47). This model of inflation is particularly interesting, as it predicts primordial gravitational waves (GWs) with a strength comparable to that of the present observational bound (2, 47).

2.1.2. Axion dark matter. Light axions are compelling candidates for DM. The most straightforward way to produce axion DM would be the misalignment mechanism (11–14). In the early Universe, the initial value of the axion field is generically misaligned from the present vacuum value, which can be parametrized as

$$a(t_i) - a(t_0) = \Theta_{\rm in}\frac{f_a}{N_{\rm DW}}, \tag{9.}$$

where t_0 is the present time and $\Theta_{\rm in}$ is an angle parameter in the range $[0, \pi]$. Due to Hubble friction, the axion field has negligible evolution when the Hubble expansion rate $\mathcal{H}(t) \gg m_a(t)$. In the later time $t = t_{\rm osc}$ when $\mathcal{H}(t_{\rm osc}) \sim m_a(t_{\rm osc})$, the axion field begins to oscillate around the present vacuum value, and the axion energy density ρ_a subsequently evolves like matter energy density. If one takes the simple harmonic approximation for the axion potential, the resulting axion DM abundance is (14)

$$\Omega_a(t_0)h^2 \simeq 0.1\left[\frac{m_a(t_0)}{\rm eV}\right]^{1/2}\left[\frac{m_a(t_0)}{m_a(t_{\rm osc})}\right]^{1/2}\left(\frac{\Theta_{\rm in} f_a/N_{\rm DW}}{3\times 10^{11}\,{\rm GeV}}\right)^2, \tag{10.}$$

where $\Omega_a(t_0) = \rho_a(t_0)/\rho_c(t_0)$ $[\rho_c(t_0) = 3M_P^2\mathcal{H}(t_0)^2]$, and h is defined by $\mathcal{H}(t_0) = 100h$ km s^{-1} Mpc^{-1}.

For the QCD axion, $m_a(t_0) \approx f_\pi m_\pi/(f_a/N_{\rm DW})$ (see Equation 28) and $m_a(t_{\rm osc})/m_a(t_0) \approx 6 \times 10^{-4}({\rm GeV}/T_{\rm osc})^n$ ($n \simeq 4$) for $T_{\rm osc} \gtrsim 150$ MeV (48), where m_π and f_π are the pion mass and the pion decay constant, respectively, and $T_{\rm osc}$ is the temperature at $t = t_{\rm osc}$. Inserting these into Equation 10, one finds the following relic abundance of the QCD axion (11–13):

$$\left[\Omega_a(t_0)h^2\right]_{\rm QCD} \simeq 0.1\,\Theta_{\rm in}^2 \left(\frac{f_a/N_{\rm DW}}{10^{12}\,{\rm GeV}}\right)^{(n+3)/(n+2)} \quad (n \simeq 4). \tag{11.}$$

Another interesting example is ultralight ALP DM with $m_a(t_{\rm osc}) = m_a(t_0)$ (14, 49). Unlike the QCD axion, m_a and $f_a/N_{\rm DW}$ for such an ALP can be regarded as independent parameters, so its relic abundance is given by

$$\left[\Omega_a(t_0)h^2\right]_{\rm ALP} \simeq 0.1\,\Theta_{\rm in}^2 \left[\frac{f_a/N_{\rm DW}}{10^{17}\,{\rm GeV}}\right]^2 \left(\frac{m_a}{10^{-22}\,{\rm eV}}\right)^{1/2}. \tag{12.}$$

2.1.3. Relaxion. In the relaxion scenario, the Higgs boson mass is relaxed down to the weak scale by the cosmological evolution of an axion-like field termed the relaxion, providing a new solution to the weak scale hierarchy problem (10). The relaxion potential takes the form

$$\begin{aligned} V &= V_0(\theta) + \mu_H^2(\theta)|H|^2 + V_{\rm br}(\theta) \\ &= -\Lambda^4\cos(N_{\rm DW}\theta) + \left[\Lambda_H^2 + \Lambda_1^2\cos(N_{\rm DW}\theta)\right]|H|^2 - \Lambda_{\rm br}^4(H)\cos(N_{\rm br}\theta + \alpha), \end{aligned} \tag{13.}$$

where $\theta = a/f_a \cong \theta + 2\pi$ ($N_{\rm DM}, N_{\rm br} \in \mathbb{Z}$) and H is the Higgs doublet field in the SM whose observed vacuum expectation value is given by $v = \sqrt{2}\langle|H|\rangle = 246$ GeV. Λ_H ($\gg v$) is the cutoff scale for the Higgs boson mass, and $\Lambda_{\rm br}(H)$ is a Higgs-dependent scale parameter that becomes nonzero once H develops a nonzero vacuum value. Here the terms involving $\cos(N_{\rm DW}\theta)$ are generated at high scales around the cutoff scale, so naturally, $\Lambda \sim \Lambda_1 \sim \Lambda_H \gg v$. In contrast, the barrier potential $V_{\rm br} = -\Lambda_{\rm br}^4(H)\cos(N_{\rm br}\theta + \alpha)$ is generated at a lower scale around or below v so that $\Lambda_{\rm br} \equiv \Lambda_{\rm br}(v) \lesssim v$.

Initially, the effective Higgs mass $\mu_H^2(\theta) = \Lambda_H^2 + \Lambda_1^2\cos(N_{\rm DW}\theta)$ is supposed to have a large value $\mu_H^2[\theta(t_i)] \sim \Lambda_H^2 > 0$. But it is subsequently relaxed down to $\mu_H^2[\theta(t_f)] \sim -v^2 < 0$ by the relaxion field excursion $a(t_i) - a(t_f) \sim f_a/N_{\rm DW}$ driven by the potential V_0. Since a nonzero $V_{\rm br}$ is developed after the relaxion passes through the critical point $\mu_H^2(\theta) = 0$, the relaxion is finally stabilized by the competition between the sliding slope $\partial_\theta V_0$ and the barrier slope $\partial_\theta V_{\rm br}$, which requires

$$\frac{N_{\rm br}}{N_{\rm DW}} \sim \frac{\Lambda^4}{\Lambda_{\rm br}^4} \gtrsim \frac{\Lambda_H^4}{v^4}. \tag{14.}$$

For successful stabilization, the scheme also requires a mechanism to dissipate the relaxion kinetic energy. In the original model (10), such dissipation occurs by Hubble friction over a long period of inflationary expansion. Some alternative possibilities are discussed in Section 3.1.2 in connection with the relaxion coupling hierarchy.

2.2. Axion Couplings to the Standard Model

To discuss axion couplings to the SM, it is convenient to use the angular field

$$\theta(x) = \frac{a(x)}{f_a} \cong \theta(x) + 2\pi \tag{15.}$$

in the field basis for which only the axion transforms under PQ symmetry (Equation 4) and all the SM fields are invariant (50). Here we are interested in axions with $m_a < v \ll f_a$. We thus start with an effective Lagrangian defined at the weak scale, which could be derived from a more fundamental theory defined at higher energy scale. Then the PQ-invariant part of the Lagrangian is given by

$$\mathcal{L}_0 = \frac{1}{2} f_a^2 \partial_\mu \theta \partial^\mu \theta + \sum_\psi c_\psi \partial_\mu \theta \bar{\psi} \bar{\sigma}^\mu \psi, \tag{16.}$$

where $\psi = (Q, u^c, d^c, L, e^c)$ denote the chiral quarks and leptons in the SM and derivative coupling to the Higgs doublet current $i(H^\dagger \partial_\mu H - \partial_\mu H^\dagger H)$ is rotated away by an axion-dependent $U(1)_Y$ transformation. Generically, c_ψ can include flavor-violating components, but we assume that such components are negligible.

The PQ-breaking part includes a variety of nonderivative axion couplings such as

$$\begin{aligned} \Delta\mathcal{L} = & \frac{\theta(x)}{32\pi^2} \left(c_G G^{\alpha\mu\nu} \widetilde{G}^\alpha_{\mu\nu} + c_W W^{i\mu\nu} \widetilde{W}^i_{\mu\nu} + c_B B^{\mu\nu} \widetilde{B}_{\mu\nu} \right) \\ & - V_0(\theta) - \mu_H^2(\theta) |H|^2 + \cdots, \end{aligned} \tag{17.}$$

where $F^X_{\mu\nu} = (G^\alpha_{\mu\nu}, W^i_{\mu\nu}, B_{\mu\nu})$ are the $SU(3)_c \times SU(2)_W \times U(1)_Y$ gauge field strengths, $\widetilde{F}^X_{\mu\nu} = \frac{1}{2}\epsilon_{\mu\nu\rho\sigma} F^{X\rho\sigma}$ are their duals, and the ellipsis stands for PQ-breaking axion couplings to operators with mass dimension ≥ 4 other than $F^X_{\mu\nu} \tilde{F}^{X\mu\nu}$, which we ignore in the following discussion. We assume that the underlying theory does not generate an axion monodromy (51), so the theory allows for a field basis for which each term in $\Delta\mathcal{L}$, or $e^{iS_{\rm int}}$ of the corresponding action $S_{\rm int}$, is invariant under $\theta \to \theta + 2\pi$. In such a field basis, V_0 and μ_H^2 are 2π periodic functions of θ, c_G and c_W are integers, and c_B is a rational number. Although the first line of Equation 17 includes $a(x)$, this coupling depends only on the derivative of $a(x)$ in perturbation theory since $F^X_{\mu\nu} \tilde{F}^{X\mu\nu}$ is a total divergence. As a consequence, these terms contribute to the renormalization group (RG) running of the derivative couplings to the SM fermions in Equation 16 (52, 53); e.g.,

$$\frac{dc_\psi}{d\ln\mu} = -\sum_{X=G,W,B} \frac{3}{2} \left(\frac{g_X^2}{8\pi^2} \right)^2 \mathbb{C}_X(\psi) \Big[c_X - 2 \sum_{\psi'} c_{\psi'} \mathbb{T}_X(\psi') \Big] \tag{18.}$$

at scales above the weak scale, where $\mathbb{C}_X(\psi)$ and $\mathbb{T}_X(\psi)$ are the quadratic Casimir and Dynkin index of ψ. Some axion models predict $c_\psi = 0$ at the UV scale (39, 40). In such models, the low-energy values of c_ψ are determined mainly by their RG evolution, including the effect of Equation 18 (52, 53).

To examine the phenomenological consequences, one may scale down the weak scale Lagrangians (Equations 16 and 17) to lower energy scales. This procedure is straightforward, at least at scales above the QCD scale. It is worth briefly discussing how PQ breaking by $\partial_\theta \mu_H^2$ is transmitted to low-energy physics, which is particularly relevant for the low-energy phenomenology of the relaxion (18–20). After electroweak symmetry breaking, a nonzero value of $\partial_\theta \mu_H^2$ results in PQ- and CP-breaking Higgs-axion mixing, with the mixing angle

$$\sin\theta_{ab} \simeq \langle \partial_\theta \ln \mu_H(\theta) \rangle \frac{v}{f_a}. \tag{19.}$$

Mixing also gives rise to the axion-dependent masses of the SM fermions and gauge bosons:

$$\sum_{\Psi} m_{\Psi}(\theta)\bar{\Psi}\Psi + M_W^2(\theta)W^{\mu+}W_{\mu}^{-} + \frac{1}{2}M_Z^2(\theta)Z^{\mu}Z_{\mu}, \qquad 20.$$

with $\partial_\theta \ln M_\Phi(\theta) = \partial_\theta \ln v(\theta) = \partial_\theta \ln \mu_H(\theta)$ $(M_\Phi = m_\Psi, M_W, M_Z)$, where the Dirac fermion Ψ denotes the SM quarks and charged leptons and $v(\theta) = [-\mu_H^2(\theta)/\lambda_H]^{\frac{1}{2}}$ is the axion-dependent Higgs vacuum value with the Higgs quartic coupling λ_H, which is independent of the axion field in our approximation. Then, integrating out the gauge-charged heavy field Φ leaves an axion-dependent threshold correction to the low-energy gauge couplings as

$$\Delta g = \Delta\beta_g(M_\Phi)\ln[M_\Phi(\theta)/\mu], \qquad 21.$$

where $\Delta\beta_g(M_\Phi)$ is the threshold correction to the beta function at the scale $\mu \sim M_\Phi$.

Scaling the theory down to $\mu \sim 1$ GeV, the axion effective Lagrangian is given by

$$\begin{aligned}\mathcal{L} = &\frac{1}{2}f_a^2\partial_\mu\theta\partial^\mu\theta + \sum_{\Psi=q,\ell} c_\Psi \frac{\partial_\mu\theta}{2}\bar{\Psi}\gamma^\mu\gamma_5\Psi \; + \frac{\theta(x)}{32\pi^2}\left(c_G G^{\alpha\mu\nu}\widetilde{G}^{\alpha}_{\mu\nu} + c_\gamma F^{\mu\nu}\widetilde{F}_{\mu\nu}\right)\\ &- V_0(\theta) + \frac{\mu_H^4(\theta)}{4\lambda_H} - \sum_{\Psi=q,\ell} m_\Psi(\theta)\bar{\Psi}\Psi - \frac{1}{4g_s^2(\theta)}G^{\alpha\mu\nu}G^{\alpha}_{\mu\nu} - \frac{1}{4e^2(\theta)}F^{\mu\nu}F_{\mu\nu} + \cdots, \qquad 22.\end{aligned}$$

where $q = (u, d, s)$, $\ell = (e, \mu)$, and $g_s^2(\theta), e^2(\theta)$ include the axion-dependent threshold corrections in Equation 21 from the heavy quarks and tau leptons. If the RG evolutions are ignored, c_Ψ and c_γ are determined by the weak scale parameters c_Ψ, $c_{W,B}$ in Equations 16 and 17 as

$$c_u = c_{Q_1} + c_{u_1^c}, \quad c_{d,s} = c_{Q_{1,2}} + c_{d_{1,2}^c}, \quad c_{e,\mu} = c_{L_{1,2}} + c_{e_{1,2}^c}, \quad c_\gamma = c_W + c_B. \qquad 23.$$

In our case, both $\partial_\theta m_\Psi(\theta)$ and $\partial_\theta g^2(\theta)$ originate from $\partial_\theta \mu_H^2(\theta)$. Hence, Equation 22 results in the following PQ- and CP-breaking couplings at $\mu \sim 1$ GeV:

$$\begin{aligned}&\theta(x)\left(\sum_{\Psi=q,\ell}\bar{c}_\Psi m_\Psi\bar{\Psi}\Psi + \frac{\bar{c}_G}{32\pi^2}G^{\alpha\mu\nu}G^{\alpha}_{\mu\nu} + \frac{\bar{c}_\gamma}{32\pi^2}F^{\mu\nu}F_{\mu\nu}\right),\\ &\bar{c}_\Psi = -\langle\partial_\theta \ln\mu_H(\theta)\rangle, \quad \bar{c}_G = 2\langle\partial_\theta\ln\mu_H(\theta)\rangle, \quad \bar{c}_\gamma = -\frac{5}{3}\langle\partial_\theta\ln\mu_H(\theta)\rangle. \qquad 24.\end{aligned}$$

Many of the observable consequences of axions, in particular those of light axions, are determined by couplings to hadrons or to the electron at scales below the QCD scale. Such couplings can be derived in principle from the effective Lagrangian (Equation 22) defined at $\mu \sim 1$ GeV. In the following, we present the low-energy axion couplings relevant for our subsequent discussion of axion phenomenology (1, 3). Specifically, we express the relevant 1PI couplings at low momenta $p < 1$ GeV in terms of the Wilsonian model parameters defined at the weak scale while ignoring the subleading corrections. Many couplings to hadrons can be obtained by appropriate matching between Equation 22 and the chiral Lagrangian of nucleons and light mesons (52–54). For PQ- and CP-breaking axion couplings below the QCD scale, there are two sources. One is axion coupling to the QCD anomaly combined with a nonzero value of the QCD vacuum angle $\theta_{\rm QCD} = c_G\langle\theta(x)\rangle$, and the other is Higgs-axion mixing induced by $\partial_\theta\mu_H^2(\theta) \neq 0$. For couplings

from Higgs-axion mixing, one can use the known results for the low-energy couplings of the light Higgs boson (55, 56). One then finds

$$\mathcal{L}_{\rm 1PI} = \frac{g_{a\gamma}}{4} a F^{\mu\nu}\widetilde{F}_{\mu\nu} + \frac{\bar{g}_{a\gamma}}{4} a F^{\mu\nu} F_{\mu\nu} + \sum_{\Psi=p,n,e,\mu} \left(g_{a\Psi} \frac{\partial_\mu a}{2m_\Psi} \bar{\Psi}\gamma^\mu\gamma_5\Psi + \bar{g}_{a\Psi} a \bar{\Psi}\Psi \right)$$
$$+ \frac{1}{2}\bar{g}^{(1)}_{a\pi} a \left(\partial_\mu\pi^0\partial^\mu\pi^0 + 2\partial_\mu\pi^+\partial^\mu\pi^-\right) + \frac{1}{2}\bar{g}^{(2)}_{a\pi} a \left(\pi^0\pi^0 + 2\pi^+\pi^-\right), \qquad 25.$$

where

$$g_{a\gamma} = \frac{\alpha_{\rm em}}{2\pi}\frac{1}{f_a}\Big[c_\gamma - \frac{2}{3}\frac{(4m_d+m_u)}{(m_u+m_d)}c_G - 2\sum_{\ell=e,\mu}\left(1 - A_f(\tau_\ell)\right)c_\ell\Big],$$

$$\bar{g}_{a\gamma} = \frac{\alpha_{\rm em}}{2\pi}\frac{1}{f_a}\Big[-\frac{11}{9} + \sum_{\Phi=K^\pm,\pi^\pm}\frac{11+8\tau_\Phi}{54}\bar{A}_s(\tau_\Phi) + \frac{4}{3}\sum_{\ell=e,\mu}\bar{A}_f(\tau_\ell)\Big]\langle\partial_\theta \ln\mu_H(\theta)\rangle,$$

$$g_{ap} = \frac{m_p}{f_a}(-0.47c_G + 0.88c_u - 0.39c_d), \quad g_{an} = \frac{m_n}{f_a}(-0.02c_G - 0.39c_u + 0.88c_d),$$

$$\bar{g}_{ap} = \bar{g}_{an} = \frac{m_N}{f_a}\left[-\frac{2}{9}\langle\partial_\theta \ln\mu_H(\theta)\rangle + \theta_{\rm QCD}\frac{m_u m_d}{(m_u+m_d)^2}\frac{\sigma_{\pi N}}{m_N}\right],$$

$$g_{a\ell} = c_\ell\frac{m_\ell}{f_a}, \quad \bar{g}_{a\ell} = -\langle\partial_\theta \ln\mu_H(\theta)\rangle\frac{m_\ell}{f_a} \quad (\ell = e,\mu),$$

$$\bar{g}^{(1)}_{a\pi} = \frac{4}{9}\frac{\langle\partial_\theta \ln\mu_H(\theta)\rangle}{f_a}, \quad \bar{g}^{(2)}_{a\pi} = \frac{m_\pi^2}{f_a}\left[-\frac{5}{3}\langle\partial_\theta \ln\mu_H(\theta)\rangle + \theta_{\rm QCD}\frac{m_u m_d}{(m_u+m_d)^2}\right]. \qquad 26.$$

Here we use the result of Reference 57 for g_{aN} ($N = p, n$), $\sigma_{\pi N} = \frac{1}{2}(m_u+m_d)\langle N|(\bar{u}u+\bar{d}d)|N\rangle \simeq 42$ MeV for $\bar{g}_{aN}$ (58), and ignore the contribution to $\bar{g}_{a\gamma}$ from $\theta_{\rm QCD}$. The $\theta_{\rm QCD}$ contribution to $\bar{g}_{aN}$ is obtained in the isospin symmetric limit (59) (see Reference 60 for the subleading corrections). The 1PI axion-photon couplings $g_{a\gamma}$ and $\bar{g}_{a\gamma}$ describe the processes with on-shell photons. These couplings depend on the variables $\tau_j = p_a^2/4m_j^2$, where p_a (<1 GeV) is the axion four momentum and m_j is the appropriate hadron or lepton mass. For $p_a^2 \ll m_j^2$, it is sufficient to approximate the loop functions as $A_f \simeq \bar{A}_s \simeq \bar{A}_f \simeq 1$; for the loop functions when $p_a^2 \gtrsim m_j^2$, see References 55 and 61.

Let us finally consider the axion effective potential. For the weak scale Lagrangian (Equation 17), it is obtained as

$$V_{\rm eff} = V_0(\theta) - \frac{1}{4\lambda_H}\mu_H^4(\theta) - \frac{f_\pi^2 m_\pi^2}{m_u+m_d}\sqrt{m_u^2+m_d^2+2m_u m_d\cos(c_G\theta)} + \cdots. \qquad 27.$$

On the right-hand side of Equation 27, the second term arises from electroweak symmetry breaking, and the third term is generated by low-energy QCD dynamics through axion coupling to the gluon anomaly (57). The ellipsis denotes the subleading contributions, which include, for instance, those from the PQ-breaking couplings $\bar{c}_G$ and $\bar{c}_q$ in the effective Lagrangian (Equation 24). The subleading contributions are negligible relative to the electroweak symmetry-breaking contribution in our case. For the QCD axion, the effective potential is dominated by the term induced by the gluon anomaly. More specifically, $|\partial_\theta V_0|$, $|\partial_\theta \mu_H^4|$, and the ellipsis part are assumed to be smaller

than $10^{-10} f_\pi^2 m_\pi^2$ such that the strong CP problem is solved with $|\theta_{\rm QCD}| = |c_G \langle a \rangle / f_a| \lesssim 10^{-10}$. The corresponding QCD axion mass is found by expanding Equation 27 about $\theta = 0$ and is given by

$$m_{a_{\rm QCD}} \simeq c_G \frac{f_\pi m_\pi}{f_a} \frac{\sqrt{m_u m_d}}{m_u + m_d} \simeq 5.7\ \mu{\rm eV} \left(\frac{10^{12}\ {\rm GeV}}{f_a / c_G} \right). \quad 28.$$

2.3. Theory Constraints on Axion Couplings

Studies of the quantum properties of BHs and work with string theories suggest that there are nontrivial constraints on effective field theories having a UV completion incorporating quantum gravity (62). For instance, it has been argued that, for axions in theories compatible with quantum gravity, there exist certain instantons that couple to axions with a strength stronger than that of gravity. This has been proposed as a generalization of the weak gravity conjecture (WGC) on the $U(1)$ gauge boson, which states that there exists a particle with mass m and charge Q satisfying $Q \geq m/M_P$ (25, 63). Specifically, the axion WGC (25–29) suggests that, given the canonically normalized axions $\vec{a} = (a_1, a_2, \ldots, a_N)$, there is a set of instantons $\{I\}$ with Euclidean actions $\{S_I\}$ and axion-instanton couplings

$$\vec{g}_{aI} = \left(\frac{1}{f_{I1}}, \frac{1}{f_{I2}}, \ldots, \frac{1}{f_{IN}} \right), \quad 29.$$

which would generate PQ-breaking amplitudes (for a constant background axion field)

$$\mathcal{A}_I \propto \exp(-S_I + i \vec{g}_{aI} \cdot \vec{a}), \quad 30.$$

for which the convex hull spanned by $M_P \vec{g}_{aI} / S_I$ includes the N-dimensional unit ball. This convex hull condition can also be expressed as follows. For an arbitrary linear combination of N axions, e.g., $a = \hat{u} \cdot \vec{a}$ with $|\hat{u}| = 1$, there exists an instanton I, which we term the WGC instanton, with the axion-instanton coupling satisfying[2]

$$g_{a{\rm WGC}} \equiv |\hat{u} \cdot \vec{g}_{aI}| \gtrsim \frac{S_I}{M_P}. \quad 31.$$

For axions from p-form gauge fields in string theory, this bound is often saturated by couplings to the corresponding brane instantons (4, 44, 45, 64).

To examine the implications of the axion WGC, one sometimes assumes that the axion-instanton couplings that span the convex hull satisfying the condition in Equation 31 also generate the leading terms in the axion potential (27–29, 65–67). However, this assumption appears to be too strong to be applicable for generic cases. Generically, the axion potential depends on many features of the model other than the couplings and Euclidean actions of WGC instantons that are constrained as in Equation 31. In this regard, it is plausible that some of the leading terms in the axion potential are generated by certain dynamics other than WGC instantons, e.g., confining YM dynamics, additional instantons whose couplings are not involved in spanning the convex hull for the WGC, or Planck scale–suppressed higher-dimensional operators for accidental $U(1)_{\rm PQ}$ (26,

[2] A model-dependent coefficient of order unity can be multiplied to this bound.

29, 30, 65). We therefore adopt the viewpoint that the axion WGC implies the existence of certain instantons (termed the WGC instantons) whose couplings span the convex hull satisfying the bound in Equation 31 while leaving the dynamical origin of the axion potential as an independent feature of the model.

The axion WGC bound in Equation 31 can be written in a form useful for ultralight axions. For this, let us parameterize the axion potential induced by the WGC instanton as

$$\delta V_{\rm WGC} = M_P^2 \Lambda_I^2 e^{-S_I} \cos\left(N_{\rm WGC} \frac{a}{f_a}\right), \tag{32.}$$

where Λ_I is a model-dependent scale parameter and $N_{\rm WGC}$ is an integer that characterizes axion coupling to the WGC instanton, $g_{a\rm WGC} = N_{\rm WGC}/f_a$. This potential may or may not be the leading term in the axion potential. At any rate, it provides a lower bound on the axion mass:

$$m_a^2 \gtrsim e^{-S_I} N_{\rm WGC}^2 M_P^2 \Lambda_I^2 / f_a^2, \tag{33.}$$

implying $S_I \gtrsim 2\ln(\Lambda_I/m_a)$ and therefore

$$g_{a\rm WGC} \gtrsim \frac{2\ln(\Lambda_I/m_a)}{M_P}. \tag{34.}$$

One may further assume that the WGC instanton gives nonperturbative superpotential in the context of supersymmetry, which often happens in explicit string models (49, 64, 68). This additional assumption leads to

$$\Lambda_I^2 \sim m_{3/2} M_P, \tag{35.}$$

where $m_{3/2}$ is the gravitino mass.

2.4. Observational Constraints on Axion Couplings

Low-energy axion couplings are subject to constraints from various laboratory experiments and astrophysical or cosmological observations. They can also be tested by a number of planned experiments. In this section, we summarize those constraints and the sensitivities of these planned experiments, with a focus on those relevant for axion coupling hierarchies. More comprehensive reviews of related subjects can be found in References 21–24.

2.4.1. Nongravitational probes. CP-conserving axion-photon coupling $g_{a\gamma}$ has been most widely studied for experimental searches for axions. **Figure 1*a*** summarizes the current bounds and future experimental reach for $g_{a\gamma}$ over the vast range of axion mass m_a. Axion haloscopes [resonant cavities (69–72), ABRACADABRA (73), optical ring cavity (74), TOORAD (75); see also Reference 76 for a recent proposal] are based on the hypothesis that axions constitute (a certain fraction of) DM in our Universe. For axion DM density ρ_a, the goal is to detect electromagnetic waves arising from the axion-induced effective current

$$g_{a\gamma}\partial_t a(t)\vec{B} \approx g_{a\gamma}\sqrt{2\rho_a}\sin(m_a t)\vec{B}. \tag{36.}$$

The projected sensitivity limits in **Figure 1** are obtained when $\rho_a = \rho_{\rm DM} \simeq 0.4\,{\rm GeV/cm^3}$. Otherwise, the limits are to be scaled by the factor $\sqrt{\rho_a/\rho_{\rm DM}}$. For comparison, we also display the predicted values of $g_{a\gamma} \sim (\alpha_{\rm em}/2\pi)(c_\gamma/f_a)$ for two specific type of axions with $c_\gamma/N_{\rm DW} = 1, 10^2, 10^4$:

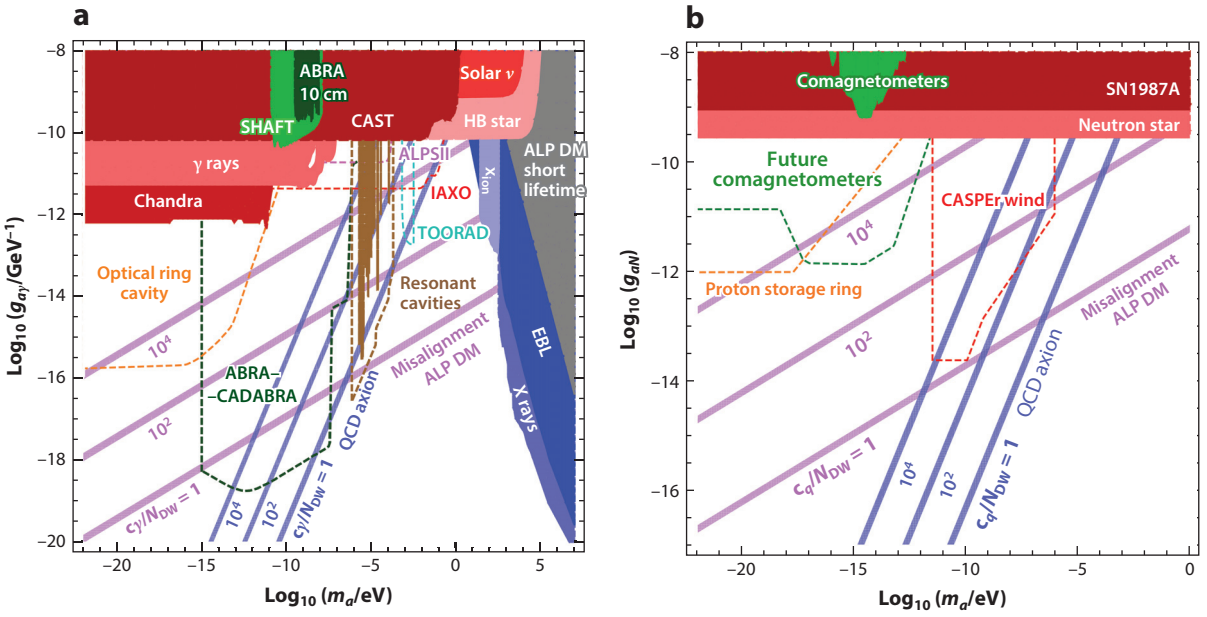

Figure 1

Constraints and future probes on (*a*) axion-photon coupling $g_{a\gamma}$ and (*b*) axion-nucleon coupling g_{aN}. The shaded regions are excluded by the existing laboratory, astrophysics, and cosmology bounds, and the dashed lines show the sensitivities of the planned experiments. We also depict $g_{a\gamma}$ and g_{aN} of ALP DM (*pink*) and the QCD axion (*blue*) for three different values of $c_\gamma/N_{\rm DW}$ and $c_q/N_{\rm DW}$, where $N_{\rm DW} = c_G$ for the QCD axion. Abbreviations: ABRA 10 cm, ABRACADABRA 10 cm; ABRACADABRA, A Broadband/Resonant Approach to Cosmic Axion Detection with an Amplifying B-field Ring Apparatus; ALP, axion-like particle; ALPSII, Any Light Particle Search II; CASPEr, Cosmic Axion Spin Precession Experiment; CAST, CERN Axion Solar Telescope; Chandra, Chandra X-Ray Observatory; DM, dark matter; EBL, extragalactic background light; HB, horizontal branch; IAXO, International Axion Observatory; QCD, quantum chromodynamics; SHAFT, Search for Halo Axions with Ferromagnetic Toroids; solar ν, solar neutrino; TOORAD, Topological Resonant Axion Detection; $x_{\rm ion}$, ionization of primordial hydrogen. Panel *a* adapted from Reference 77 (public domain) and Reference 78 (with permission), with additional data from References 73–75 and 79–84. Panel *b* adapted from Reference 77 (public domain), with additional data from References 85–88.

first, ALP DM with $\rho_a = \rho_{\rm DM}$ given by Equation 12 with $\Theta_{\rm in} = 1$, which is produced by the misalignment mechanism, and second, the QCD axion. We do not specify the cosmological relic abundance of the QCD axion, since the corresponding lines can be determined by Equation 28 without additional information. Our result shows that for both ALP DM and the QCD axion, the parameter region more easily accessible by ongoing or planned experiments has $c_\gamma/N_{\rm DW} \gg 1$, which parameterizes the hierarchy between $g_{a\gamma} \sim (\alpha_{\rm em}/2\pi)(c_\gamma/f_a)$ and the coupling $g_{a\Lambda} = N_{\rm DW}/f_a$ to generate the leading axion potential ($N_{\rm DW} = c_G$ for the QCD axion).

A similar plot for axion-nucleon coupling g_{aN} is given in **Figure 1*b***, including experimental sensitivities and the predicted coupling for ALP DM and the QCD axion with $c_q/N_{\rm DW} = 1, 10^2, 10^4$. The relevant experiments are CASPEr Wind (85), comagnetometers (86, 87), and proton storage ring (88). The goal of these experiments is to find the axion DM-induced effective magnetic field interacting with nucleon spin, whose strength is proportional to

$$g_{aN}\vec{\nabla}a(t,\vec{x}) \approx g_{aN}\sqrt{2\rho_a}\vec{v}\sin\left(m_a t - m_a\vec{v}\cdot\vec{x}\right), \qquad 37.$$

where $\vec{v}$ ($|\vec{v}| \sim 10^{-3}$) is the axion DM virial velocity with respect to the Earth. Again, the sensitivity limit in **Figure 1** is obtained for $\rho_a = \rho_{\rm DM}$, so it has to be scaled by the factor $\sqrt{\rho_a/\rho_{\rm DM}}$ otherwise. We see that the ALP parameter region more easily probed by those experiments has

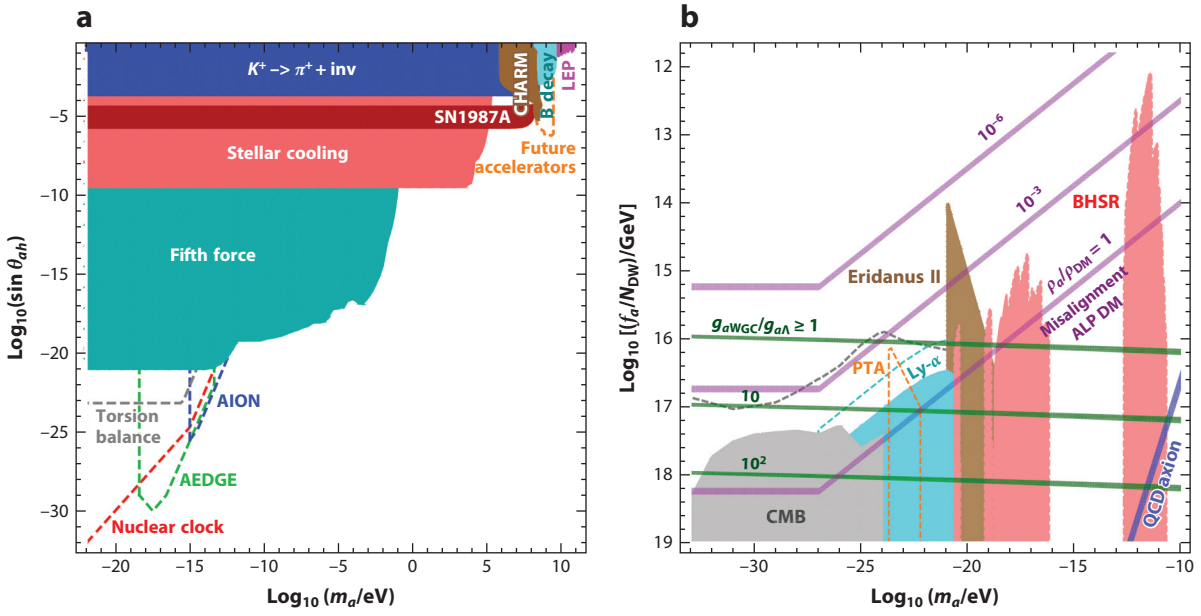

Figure 2

Constraints on (*a*) Higgs-axion mixing θ_{ab} from experimental and astrophysical probes on CP-violating axion couplings and (*b*) the axion scale f_a/N_{DW} from gravitational probes. The shaded regions are excluded by the existing constraints, while the dashed lines show the sensitivities of future experiments. For the plot in panel *b*, f_a/N_{DW} is identified as the field excursion Δa for ALP DM or dark energy, while f_a/N_{DW} is associated with the axion self-interaction strength for BHSR. (For a given mass, the lower f_a/N_{DW}, the stronger is the axion self-interaction.) We also show the axion coupling hierarchy implied by the WGC (*green*). Abbreviations: AEDGE, Atomic Experiment for Dark Matter and Gravity Exploration; AION, Atom Interferometer Observatory and Network; ALP, axion-like particle; BHSR, black hole superradiance; CHARM, CERN-Hamburg-Amsterdam-Rome-Moscow collaboration experiment; CMB, cosmic microwave background; DM, dark matter; Eridanus II, Eridanus II dwarf galaxy; LEP, Large Electron-Positron Collider; Ly-α, Lyman-α forest; PTA, pulsar timing array; QCD, quantum chromodynamics; WGC, weak gravity conjecture. Panel *a* adapted from Reference 20 (CC BY 4.0), with additional data from References 90, 91, and 95–98. Data in panel *b* from References 102–108 and 114–116.

$c_q/N_{\text{DW}} \gg 1$, representing the hierarchy between $g_{aN} \sim c_q m_N/f_a$ and $g_{a\Lambda} = N_{\text{DW}}/f_a$. Although not shown in **Figure 1**, the QUAX experiment recently excluded axion-electron coupling $g_{ae} \gtrsim 2 \times 10^{-11}$ for $m_a \simeq 43$ μeV (89), which would correspond to $c_e/N_{\text{DW}} \gtrsim 10^4$ for the QCD axion.

There are also a number of bounds and experimental probes on CP-violating axion couplings. As described in Section 2.2, such couplings can be induced predominantly by Higgs-axion mixing (Equation 19), which is indeed the case for the relaxion (18–20). We thus summarize in **Figure 2*a*** the available constraints on and future prospects for CP-violating axion couplings in terms of the Higgs-axion mixing angle θ_{ab}. Exhaustive reference lists for those constraints and future sensitivity limits can be found in References 18–20 and 92. For axions lighter than the megaelectronvolt scale, the constraints are from the axion-mediated fifth force induced by $\bar{g}_{aN}$, stellar cooling by $\bar{g}_{ae}$ (93), and supernova (SN1987A) cooling by $\bar{g}_{aN}$. The currently unconstrained supernova trapping window between 100 keV and 30 MeV may be explored by the GANDHI experiment (94). Ultralight axion DM can be tested by a future nuclear clock experiment (20), torsion balances (95), and atom interferometers such as AION (96) and AEDGE (97) through axion DM's CP-violating couplings. These experiments will probe axion DM–induced oscillations of fundamental constants like electron mass, nucleon mass, and the fine structure constant via the CP-violating couplings in Equation 25. So experimental sensitivities are proportional to the background axion DM field

$a(t,x) \approx \sqrt{2\rho_a}/m_a \cos(m_a t)$. The sensitivity lines in **Figure 2** are again obtained for $\rho_a = \rho_{\rm DM}$. In contrast, axions heavier than the megaelectronvolt scale are constrained by the CHARM beam dump experiment, rare meson decays ($K \to \pi + a\,[a \to \text{inv}]$, $B \to K + a\,[a \to \mu\mu]$), and LEP ($e^+e^- \to Z \to Za$). Heavy axions around the gigaelectronvolt scale are to be probed by various future accelerator experiments searching for long-lived particles such as FASER, CODEX-b, SHiP, and MATHUSLA (98). For the QCD axion, the dominant source of CP violation is a nonzero $|\theta_{\rm QCD}| < 10^{-10}$, which may be too tiny to be probed by the current experiments. Yet the ARIADNE experiment (99, 100) plans to probe $\theta_{\rm QCD}$ several orders of magnitude below 10^{-10} by observing the axion-mediated monopole-dipole force $\propto \bar{g}_{aN} g_{aN}$.

2.4.2. Gravitational probes. Gravitational constraints provide a complementary probe of axions. Whereas the nongravitational probes described in Section 2.4.1 constrain axions with relatively heavier masses and stronger couplings, gravitational probes can constrain extremely light axions with large, nearly Planckian, values of $f_a/N_{\rm DW}$. Such ultralight axions may constitute a substantial amount of dark energy (DE) or DM, as suggested by Equation 12, while having a large de Broglie wavelength, which can have significant cosmological and astrophysical implications. The relevant axion mass range can be classified by three windows: (*a*) a DE-like window, $m_a \lesssim 10^{-27}$ eV; (*b*) an ultralight DM window, $10^{-27}\,\text{eV} \lesssim m_a \lesssim 10^{-19}\,\text{eV}$; and (*c*) a BH superradiance window, $10^{-21}\,\text{eV} \lesssim m_a \lesssim 10^{-11}\,\text{eV}$, which has some overlap with the second window. In **Figure 2*b***, we depict the existing constraints on and expected future limits of gravitational probes of ultralight DE-like or DM axions produced by the initial misalignment $\Delta a = f_a/N_{\rm DW}$, as well as regions excluded by BH axion superradiance.

For the DE-like window $m_a \lesssim 10^{-27}$ eV, the axion field begins to oscillate after the matter-radiation equality and acts as an early DE component. As a result, the locations of the CMB acoustic peaks shift to larger angular scales (lower ℓ), and the Universe gets younger. The early DE development also increases the largest-scale anisotropies through the Integrated Sachs-Wolfe effect (101). The change in the CMB acoustic peaks and the largest-scale anisotropies constrain the axion energy density by the CMB observations, as depicted in **Figure 2*b***. For $m_a \lesssim 10^{-32}$ eV, the effect of axions on the CMB becomes almost indistinguishable from the cosmological constant within the current precision, so the constraint is weakened. If $m_a \lesssim 10^{-33}$ eV, the axion field rolls slowly to this day and behaves like standard DE.

For the ultralight DM window $10^{-27}\,\text{eV} \lesssim m_a \lesssim 10^{-19}\,\text{eV}$, the axion oscillates before the matter-radiation equality but has a cosmic size of the de Broglie wavelength, which would affect cosmic structure formation. There are a number of constraints on this mass range from the CMB (102–104), a pulsar timing array (PTA) (105), the Lyman-α forest (106, 107), and an ultrafaint dwarf galaxy (Eridanus II) (108), which are depicted in **Figure 2*b***. If $10^{-27}\,\text{eV} \lesssim m_a \lesssim 10^{-25}\,\text{eV}$, the height of the CMB acoustic peaks becomes higher than that of the ΛCDM because the axion behaves like DE until the time frame close to recombination. Moreover, the wavelike property of axion DM suppresses density perturbation below a certain comoving Jeans scale (2, 109), affecting the gravitational lensing of the CMB (110). Those effects are undiscernible for $m_a \gtrsim 10^{-25}$ eV with the current data precision, lifting the CMB constraint. The effects of axion DM on small scales are still significantly constrained by Lyman-α forest data (106, 107) and by the evolution of the dwarf galaxy Eridanus II (108), extending the excluded region up to $m_a \lesssim 10^{-19}$ eV. While the Parkes PTA currently puts only a weak constraint on the time-oscillating pressure of axion DM, it may eventually probe the projected sensitivity limit in Figure 2*b* with a 10-year data set (105).

For the BH superradiance window $10^{-21}\,\text{eV} \lesssim m_a \lesssim 10^{-11}\,\text{eV}$, observations of spinning BHs and GWs can constrain the existence of axions (5, 111). Let us briefly discuss some of the

underlying physics of this issue (for details, see Reference 112). Superradiance is a phenomenon in which incident waves (or bosonic particles) are amplified by extracting energy and angular momentum from a rotating medium. For axion superradiance, a rotating BH provides such a medium. Moreover, because of gravitational attraction, the emitted axions can form a bound state around the BH, termed the axion cloud. The axion cloud provides a continuous source of incident axions and can cause exponential growth of the axion cloud by extracting a substantial fraction of the angular momentum of the BH. In fact, such an amplification of the axion cloud is efficient only when the size of the axion cloud $r_a = (\alpha_g m_a)^{-1}$ ($\alpha_g \equiv G_N M_{\rm BH} m_a$) is comparable to the BH size $r_{\rm BH} = G_N M_{\rm BH}$, so efficient amplification occurs only for the axion mass window $m_a \sim (0.1\text{–}1) r_{\rm BH}^{-1}$. Therefore, the observations of highly spinning stellar BHs with $M_{\rm BH} = \mathcal{O}(10 M_\odot)$, supermassive BHs with $M_{\rm BH} = \mathcal{O}(10^6\text{–}10^8 M_\odot)$, and the recently observed spinning M87* with mass $6.5 \times 10^9 M_\odot$ provide strong constraints on the existence of axions with masses of 10^{-13}–10^{-11} eV, 10^{-19}–10^{-16} eV, and 10^{-21}–10^{-20} eV, respectively. The axion cloud is not absolutely stable. It can emit quasi-monochromatic GWs through axion pair annihilations or level transitions. Then the axion mass range 10^{-13}–10^{-12} eV is also ruled out by the nonobservation of this GW signal in LIGO/Virgo data.

The above exclusions assume that superradiant axion modes can grow unhindered to a large enough value. However, axions generically have a self-interaction provided by the potential, e.g., the quartic coupling $\lambda_a \sim -m_a^2 N_{\rm DW}^2 / f_a^2$ for Equation 5, which may interrupt the growth of axion modes at certain points. If this self-interaction is strong enough, the axion cloud can collapse into the BH before a significant portion of the angular momentum is extracted, creating a GW/axion burst termed a bosenova (111). Numerical simulations and perturbative estimations indicate that a bosenova occurs for $f_a/N_{\rm DW} \lesssim \left(\Delta J / G_N M_{\rm BH}^2\right)^{1/2} \alpha_g^{3/2} M_P$, where ΔJ ($\leq G_N M_{\rm BH}^2$) is the extracted angular momentum of the BH before the collapse. Then, parts of the axion cloud are blown away in the form of GW/axion burst, and the axion cloud will grow again and collapse at some point. If this cycle is repeated many times during the dynamical timescale of the BH, the whole process may take away a large portion of the BH angular momentum. Also, even before the bosenova is triggered, axion quartic coupling may prevent exponential growth of the axion cloud and cause early saturation by efficient energy transfer from the superradiant mode to the damped mode (113, 114). Given those roles of self-interaction, the condition for extracting a sizable amount of the BH angular momentum is approximately given by (114–116)

$$\mathcal{O}(10^{15}\text{–}10^{16}\,{\rm GeV}) \min\left[1, \left(10^{-18}\,{\rm eV}/m_a\right)^{1/2}\right] \lesssim f_a/N_{\rm DW}. \qquad 38.$$

When axion quartic coupling is weak enough to satisfy Equation 38, the axion parameters are excluded by BH superradiance, as in **Figure 2*b***. However, the BH superradiance bounds can be avoided if the axion has a hierarchically large coupling to other fields, causing early saturation of the growth of the axion cloud (117, 118). This early saturation can be due to axion–dark photon coupling $g_{aγ'} \gg g_{a\Lambda} = N_{\rm DW}/f_a$, which is technically natural and can arise from the clockwork mechanism discussed in Section 3.2.

For ultralight DE-like or DM axions, the gravitational probes can reach to a nearly Planckian value of $f_a/N_{\rm DW}$. The corresponding coupling $g_{a\Lambda} = N_{\rm DW}/f_a$ might be significantly weaker than axion-instanton coupling $g_{a\rm WGC}$, which is bounded as Equation 31 by the WGC. To see this, we use Equations 34 and 35 with $m_{3/2} \gtrsim 10$ TeV for the bound on $g_{a\rm WGC}$, use Equation 12 with $\Theta_{\rm in} = 1$ for the ALP DM density determined by m_a and $g_{a\Lambda} = N_{\rm DW}/f_a$, and display the resulting $g_{a\rm WGC}/g_{a\Lambda}$ in **Figure 2*b***. The observation of a signal below the line of $g_{a\rm WGC}/g_{a\Lambda} \geq 1$ would challenge the assumption that axion potential is predominantly generated by the WGC instanton. However, this observation is compatible with the axion WGC, which implies the existence of a certain instanton

with coupling $g_{a\mathrm{WGC}} \gtrsim S_I/M_P$ while leaving $g_{a\Lambda} < g_{a\mathrm{WGC}}$ as an open possibility. Our results show that future CMB and PTA observations can probe the region with $g_{a\mathrm{WGC}}/g_{a\Lambda} \geq 10$.

3. AXIONS WITH HIERARCHICAL COUPLINGS

An interesting feature of axions is that there can be technically natural hierarchies among the couplings of a given axion. Moreover, those hierarchies can have observable consequences. We have seen that, since axions are a periodic field, their PQ-breaking couplings are given in terms of integers; for example, $g_{a\Lambda} = N_{\mathrm{DW}}/f_a$. Then the ratios of those quantized couplings do not receive quantum correction. As a consequence, any hierarchy among the PQ-breaking couplings of a given axion can be technically natural, although it may require an explanation for its origin. Additionally, the approximate $U(1)_{\mathrm{PQ}}$ symmetry assures that PQ-conserving couplings can be much stronger than PQ-breaking couplings without causing a fine-tuning problem. In this section, we present some examples of well-motivated axion coupling hierarchies and discuss the model-building attempts to achieve those hierarchies in low-energy effective theory.

3.1. Examples

There are various well-motivated examples of axion coupling hierarchies. Here we present some of those examples.

3.1.1. Coupling hierarchies for laboratory searches for axions. Our first example is coupling hierarchies relevant for laboratory searches for axions. We discuss in Section 2.4.1 (see **Figure 1**) that the parameter region of ALP DM or the QCD axion that is more easily accessible by ongoing or planned experiments has a bigger hierarchy between g_{aX} ($X = \gamma, N$) and $g_{a\Lambda}$, where $g_{a\Lambda} = N_{\mathrm{DW}}/f_a$ is coupling to generate the leading axion potential. To see this, we use Equations 12, 26, and 28 and find

$$g_{aX} \sim \begin{cases} 3 \times 10^{-12} R_X \left(\frac{m_a}{\mathrm{eV}}\right)^{1/4} \left(\frac{0.1\Theta_{\mathrm{in}}^2}{\Omega_a h^2}\right)^{1/2} \mathrm{GeV}^{-1} & \text{(ALP dark matter)} \\ 10^{-13} R_X \left(\frac{m_a}{\mu\mathrm{eV}}\right) \mathrm{GeV}^{-1} & \text{(QCD axion)} \end{cases}, \tag{39.}$$

where

$$R_\gamma = \frac{\alpha_{\mathrm{em}}}{2\pi} \frac{\max(c_G, c_W, c_B)}{N_{\mathrm{DW}}}, \quad R_N = m_N \frac{\max(c_G, c_q)}{N_{\mathrm{DW}}}. \tag{40.}$$

The above result shows that, for a given axion mass, the corresponding g_{aX} has a bigger value for bigger R_X and so is more easily detected. These correlations between g_{aX} and m_a are displayed by the ALP DM and QCD axion lines in **Figure 1** for three different values of the hierarchy factor R_X determined by $c_\gamma/N_{\mathrm{DW}} = (c_W + c_B)/N_{\mathrm{DW}} = 1, 10^2, 10^4$ and $c_q/N_{\mathrm{DW}} = 1, 10^2, 10^4$. For ALP DM, $\rho_a = \rho_{\mathrm{DM}}$ and $\Theta_{\mathrm{in}} = 1$ are also assumed.

Another interesting possibility is that one of g_{aX} ($X = \gamma, N, e$) is much stronger than the others, e.g., (*a*) the photophilic limit with $c_{B,W} \gg c_{G,q}$ (37, 38, 119–121), (*b*) the nucleophilic limit with $c_q \gg c_{G,W,B}$ (120–122), and (*c*) the leptophilic limit with $c_e \gg c_{G,q}$ (121, 123). Since most axion search experiments are designed to be sensitive to one specific coupling, these limits may also be more easily probed by ongoing or planned experiments. Yet the natural ranges of these parameter hierarchies are limited by RG mixings between c_X ($X = G, W, B$) and c_Ψ ($\Psi = q, e$) induced by SM interactions, for instance, by the RG evolution in Equation 18. Also, at scales around the nucleon or electron mass, 1PI axion-photon coupling $g_{a\gamma}$ receives a threshold correction $\delta g_{a\gamma} = \mathcal{O}\left(\frac{\alpha_{\mathrm{em}}}{2\pi} \frac{p_a^2}{m_\Psi^2} \frac{g_{a\Psi}}{m_\Psi}\right)$ from axion-fermion coupling $g_{a\Psi}$ ($\Psi = e, N$), where p_a denotes

the axion four momentum. Taking those quantum corrections into account, we find the following naturalness bounds on the possible hierarchies among g_{aX} ($X = \gamma, N, e$):

$$\text{Photophilic limit:}\quad 1 \ll \frac{c_{W,B}}{c_{q,G}} \sim \frac{2\pi m_N}{\alpha_{\rm em}}\frac{g_{a\gamma}}{g_{aN}} \lesssim \mathcal{O}\left[\frac{4\pi^2}{\alpha_{\rm em}^2}\frac{1}{\ln(f_a/m_N)}\right],$$

$$\text{Nucleophilic limit:}\quad 1 \ll \frac{c_q}{c_{B,W,G} + \mathcal{O}(p_a^2 c_q/m_N^2)} \sim \frac{\alpha_{\rm em}}{2\pi m_N}\frac{g_{aN}}{g_{a\gamma}} \lesssim \mathcal{O}\left(\frac{m_N^2}{p_a^2}\right),$$

$$\text{Leptophilic limit:}\quad 1 \ll \frac{c_e}{c_{G,q}} \sim \frac{m_N}{m_e}\frac{g_{ae}}{g_{aN}} \lesssim \mathcal{O}\left[\frac{4\pi^2}{\alpha_{\rm em}^2}\frac{1}{\ln(f_a/m_N)}\right]. \qquad 41.$$

3.1.2. Coupling hierarchy for the relaxion. In the relaxion solution to the weak scale hierarchy problem, which is briefly described in Section 2.1.3, the technically unnatural hierarchy between $v = 246$ GeV and the Higgs mass cutoff scale Λ_H is traded for a technically natural but much bigger hierarchy between relaxion couplings. For instance, for the original model with $\Lambda_{\rm br} \lesssim v$ (10), the relaxion stabilization condition (Equation 14) leads to

$$\frac{g_{a\rm br}}{g_{a\Lambda}} = \frac{N_{\rm br}}{N_{\rm DW}} \sim \frac{\Lambda^4}{\Lambda_{\rm br}^4} \gtrsim \frac{\Lambda_H^4}{v^4}, \qquad 42.$$

where $g_{a\Lambda} = N_{\rm DW}/f_a$ and $g_{a\rm br} = N_{\rm br}/f_a$ are the relaxion couplings to generate V_0 and $V_{\rm br}$ in the relaxion potential (Equation 13).

A similar hierarchy is required for different models that exploit different mechanisms to dissipate away relaxion kinetic energy (124–130). Here we consider two examples in which dissipation is dominated by bosonic particle production (125, 130). The relaxion initial velocity can be greater than the barrier height (i.e., $\dot{a}_0 > \Lambda_{\rm br}^2$) because Hubble friction is negligible in these examples. Yet the relaxion can efficiently lose its kinetic energy by developing nonhomogeneous modes (i.e., producing relaxion quanta), which is dubbed relaxion fragmentation (130). The relaxion will eventually be trapped at a local potential minimum when its velocity drops below the barrier height. Successful implementation of the relaxion fragmentation requires

$$\frac{g_{a\rm br}}{g_{a\Lambda}} = \frac{N_{\rm br}}{N_{\rm DW}} \sim \max\left[\frac{\Lambda^4}{\Lambda_{\rm br}^4} \times \frac{\dot{a}_0^2}{\Lambda_{\rm br}^4}, \frac{\Lambda_1^2}{v^2} \times \frac{\dot{a}_0^4}{\Lambda_{\rm br}^8}\right] \gtrsim \frac{\Lambda_H^4}{v^4}, \qquad 43.$$

with $\dot{a}_0 \gtrsim \Lambda_{\rm br}^2$ and $\Lambda_{\rm br} \lesssim v$, which is comparable to or stronger than the hierarchy in Equation 42.

Tachyonic production of light gauge bosons can also serve as friction for the relaxion (125, 130). In contrast to the above scenarios, here the Higgs vacuum value is initially $\mathcal{O}(\Lambda_H)$ and later relaxed to the observed weak scale. The relaxion is coupled to electroweak gauge bosons as in Equation 17, but with $c_W = -c_B$ to avoid coupling to the photon. Initially, the W/Z bosons are heavy, and their production is negligible. As the Higgs vacuum value is relaxed to the observed one, these bosons become light enough to be produced by the rolling relaxion, causing the relaxion to lose its kinetic energy and eventually stop the excursion. Regarding the axion coupling hierarchy, this model requires

$$\frac{g_{a\rm br}}{g_{a\Lambda}} = \frac{N_{\rm br}}{N_{\rm DW}} > \max\left[\frac{\Lambda_H^4}{\Lambda_{\rm br}^4}, \frac{\Lambda_H^2}{v^2}\right] \qquad 44.$$

for the relaxion to scan the Higgs mass with enough precision. The key difference from other scenarios is that in this case $\Lambda_{\rm br}$ is independent of the Higgs field, so it can be bigger than v. Then the above coupling hierarchy can be significantly weaker than those in other scenarios. In contrast, there can be additional coupling hierarchy in this scenario due to coupling to electroweak gauge bosons: $c_W/8\pi^2 f_a = -c_B/8\pi^2 f_a \sim v/\dot{a}_0$.

3.1.3. Coupling hierarchies for large field excursion. Our next example is the coupling hierarchy associated with the axion WGC (25–29). As discussed in Section 2.1, some well-motivated axions can have a large cosmological field excursion $\sim 1/g_{a\Lambda} = f_a/N_{\rm DW}$ comparable to M_P or even bigger. Since axion-instanton coupling $g_{a\rm WGC}$ suggested by the WGC is bounded as in Equation 31, for such axions there can be a coupling hierarchy with

$$g_{a\rm WGC} \gg g_{a\Lambda}. \qquad 45.$$

As concrete examples, one may consider (*a*) axion inflation with $f_a/N_{\rm DW} \sim \sqrt{N_e} M_P$ and $m_a \sim \mathcal{H}_{\rm inf}/\sqrt{N_e}$, which is presented in Section 2.1.1; (*b*) axion-like DE (quintessence) with $f_a/N_{\rm DW} \sim M_P$ and $m_a \sim 10^{-33}$ eV; and (*c*) ultralight ALP DM produced by the initial misalignment $\sim \Theta_{\rm in} f_a/N_{\rm DW}$, whose relic energy density is given by Equation 12. Applying the WGC bound (Equation 31) to these cases, we find

$$\frac{g_{a\rm WGC}}{g_{a\Lambda}} \gtrsim S_I \frac{f_a/N_{\rm DW}}{M_P} \sim \begin{cases} \sqrt{N_e} S_I & \text{(axion inflation)} \\ S_I & \text{(quintessence axion)} \\ \left(\frac{S_I}{20}\right)\left(\frac{10^{-22}\,\text{eV}}{m_a}\right)^{1/4}\left(\frac{\Omega_a h^2}{0.1\Theta_{\rm in}^2}\right)^{1/2} & \text{(ALP dark matter)} \end{cases}.$$

For numerical estimates of the above coupling hierarchy, one may use Equations 34 and 35 together with $m_{3/2} \sim \mathcal{H}_{\rm inf} \sim 10^{13}$ GeV during the early Universe inflation and $m_{3/2} \gtrsim 10$ TeV in the present universe.[3] One then finds that roughly $g_{a\rm WGC}/g_{a\Lambda} \gtrsim 10^2$ for axion inflation and quintessence axions, and $g_{a\rm WGC}/g_{a\Lambda} \gtrsim 10$ for ALP DM with $m_a \sim 10^{-22}$ and $\Omega_a h^2 \sim 0.1$ (131). Such ALP DM may explain the small-scale problems of the cold DM scenario (49, 109). It is also an interesting possibility that ultralight axions with $m_a \ll 10^{-22}$ constitute a small but nonnegligible fraction of DM, e.g., $\Omega_a h^2 \sim 10^{-2}$, which would leave an observable imprint in future cosmological data. Such a case also results in $g_{a\rm WGC}/g_{a\Lambda} \gg 1$. **Figure 2*b*** shows the value of $g_{a\rm WGC}/g_{a\Lambda}$ over the parameter region where the gravitational effects of ultralight ALP DM can be probed by astrophysical or cosmological observations in the near future.

3.1.4. Coupling hierarchies with other cosmological or astrophysical motivations. In addition to the examples presented above, the coupling hierarchy $g_{a\gamma} \gg \frac{\alpha_{\rm em}}{2\pi} g_{a\Lambda}$ or a similar hierarchy between $g_{a\Lambda}$ and axion coupling to dark gauge bosons has been exploited with a variety of different cosmological or astrophysical motivations. Because of space limitations, here we simply list those works without any further discussion. They include the coupling hierarchy for magnetogenesis (132–134), dissipative inflation (135, 136), chromonatural inflation (137, 138), reduced abundance of QCD axion DM (139, 140), the production of dark photon DM (141, 142), ALP–photon–dark photon oscillations to explain the tentative EDGES signal of 21-cm photons (143), avoidance of BH superradiance bounds on axion masses (118), and resonant photon emission from mergers of axion stars/oscillons (144).

3.2. Hierarchies from the Axion Landscape

In this subsection, we discuss model-building attempts to generate hierarchical axion couplings in low-energy effective theory without having hierarchical parameters in the underlying UV theory. Most of the coupling hierarchies discussed in Section 3.1 involve quantized PQ-breaking couplings and therefore involve a large integer-valued parameter, e.g., $c_{B,W} \gg 1$ for a photophilic axion and $N_{\rm br} \gg 1$ for the relaxion. Even when all UV parameters have values of order unity, such

[3] This bound on $m_{3/2}$ is chosen to avoid cosmological moduli/gravitino problems.

a large integer may appear in low-energy effective theory as a consequence of introducing a large number of fields in UV theory (32–38, 119, 138, 145–150). Yet different models can have different efficiencies; i.e., the resulting hierarchy grows differently with regard to the number of introduced fields. Here we focus on the scheme based on the axion landscape provided by the potential of many ($N_H \gg 1$) massive axions. We explain that this scheme can generate an exponential hierarchy of $\mathcal{O}(e^{N_H})$ among the effective couplings of light axions after massive axions are integrated out.

Let us start with a generic effective Lagrangian of multiple axions:

$$\mathcal{L} = \frac{1}{2} f_{ij}^2 \partial_\mu \theta^i \partial^\mu \theta^j - V(\theta^i) + \frac{k_{Xi}\theta^i}{32\pi^2} F^{X\mu\nu} \tilde{F}^X_{\mu\nu} + c_{\psi i} \partial_\mu \theta^i \bar{\psi} \bar{\sigma}^\mu \psi + \cdots, \tag{46.}$$

where $\theta^i \cong \theta^i + 2\pi$ ($i = 1, 2, \ldots, N$), k_{Xi} are integer-valued coefficients, and summation over the repeated indices i, X, ψ is understood. The axion potential V arises as a consequence of the breakdown of the PQ symmetries $[U(1)_{\rm PQ}]^N$: $\theta^i \to \theta^i + c^i$ ($c^i =$ constants). For p-form zero-mode axions such as those in Equation 3, the corresponding PQ symmetries are often broken only by nonperturbative effects (4, 44, 49, 64), yielding $V \propto e^{-b/g_*^2}$ for some coupling g_*. Violations of accidental PQ symmetries are suppressed by certain powers of $1/M_P$ (151–153), which would result in $V \propto (f/M_P)^n$ for $f \ll M_P$. These parametric relations suggest that axion potentials with different origins generically have hierarchically different sizes, yielding hierarchical axion masses. Then, at a given energy scale, some axions can be heavy enough to be frozen at their vacuum values, while the other light axions are allowed to have a dynamical evolution over their entire field range. To describe such a situation, we analyze here a simplified model in which the axion potential has two distinct scales, Λ_A and Λ_a, with $\Lambda_A \gg \Lambda_a$. The physics we describe is the same for models with a range of large and small energy scales as long as these scales are well separated. We write the axion potential, then, as

$$V = V_H + V_L = -\sum_{A=1}^{N_H} \Lambda_A^4 \cos(q_i^A \theta^i) - \sum_{a=1}^{N_L} \Lambda_a^4 \cos(p_i^a \theta^i) \quad (\Lambda_A \gg \Lambda_a), \tag{47.}$$

where $\vec{q}^A = (q_1^A, \ldots, q_N^A)$ ($A = 1, \ldots, N_H$) and $\vec{p}^a = (p_1^a, \ldots, p_N^a)$ ($a = 1, \ldots, N_L$) with $N_L = N - N_H$ are linearly independent integer-valued vectors. For simplicity, here we consider the simple cosine potentials, including only the dominant term for each linearly independent axion combination. However, our discussion does not rely on this specific potential and applies for generic periodic axion potentials. In this system, considered in the low-energy limit, the heavy axion combinations $q_i^A \theta^i$ are frozen at the vacuum state of V_H. The light degrees of freedom are given by the N_L axions parameterizing the directions that are not constrained by V_H. As we see below, the resulting effective theory of those light axions can have rich structures, including various coupling hierarchies and enlarged field ranges.[4]

The effective Lagrangian (Equation 46) is defined in the field basis for which the discrete symmetry to ensure the periodic nature of axions is given by

$$\mathbb{Z}^N : \theta^i \to \theta^i + 2\pi \ell^i \quad (\ell^i \in \mathbb{Z}). \tag{48.}$$

However, in the regime in which axion mass hierarchies become important, it is more convenient to use a different field basis minimizing mixing between axions with hierarchically different masses.

[4]If all terms in the potential (Equation 47) have a similar size, the resulting structure of the axion landscape can be very different from ours. For a discussion of such cases, see, for instance, Reference 149.

To find such a field basis, we first decompose q_i^A into the Smith normal form (154):

$$q_i^A = \sum_B \hat{U}^A{}_B \lambda_B \hat{q}_i^B, \tag{49.}$$

where $\lambda_A \in \mathbb{Z}$, $\hat{U} = [\hat{U}^A_B] \in GL(N_H, \mathbb{Z})$, $\hat{q} = [\hat{q}_i^A, \hat{q}_i^a] \in GL(N, \mathbb{Z})$. Here $\hat{U}$ and $\hat{q}$ are integer-valued and invertible matrices whose inverses are also integer valued, and therefore $|\det \hat{U}| = |\det \hat{q}| = 1$. Then the desired field basis is obtained by the $GL(N, \mathbb{Z})$ rotation,

$$\theta_H^A = \hat{q}_i^A \theta^i, \quad \theta_L^a = \hat{q}_i^a \theta^i, \tag{50.}$$

followed by the field redefinition,

$$\theta_H^A \;\to\; \theta_H^A, \quad \theta_L^a \;\to\; \theta_L^a + \hat{q}_i^a (f^{-2})^{ij} \hat{q}_j^A (f_H^2)_{AB} \theta_H^B, \tag{51.}$$

where $f_{ij}^2 (f^{-2})^{jk} = \delta_i^k$ and $(f_H^2)_{AB}$ is defined in Equation 55. With this, θ^i are parameterized as

$$\begin{aligned} \theta^i &= \hat{n}_a^i \left[\theta_L^a + \hat{q}_j^a (f^{-2})^{jk} \hat{q}_k^A (f_H^2)_{AB} \theta_H^B \right] + \hat{n}_B^i \theta_H^B \\ &= \hat{n}_a^i \theta_L^a + (f^{-2})^{ij} \hat{q}_j^A (f_H^2)_{AB} \theta_H^B, \end{aligned} \tag{52.}$$

where the integers $\hat{n}_a^i$ are given by the $N_L \times N$ submatrix of the inverse of $\hat{q}$:

$$\hat{q}^{-1} = \left[\hat{n}_A^i,\ \hat{n}_a^i \right]^T. \tag{53.}$$

Since an inverse is involved here, the integers $\hat{n}_a^i$ can be large, even when all of q_i^A are of order unity. This plays an important role below.

Applying the above parameterization to the Lagrangian (Equation 46), we obtain

$$\begin{aligned} \mathcal{L} = & \frac{1}{2} (f_L^2)_{ab} \partial_\mu \theta_L^a \partial^\mu \theta_L^b + \frac{1}{2} (f_H^2)_{AB} \partial_\mu \theta_H^A \partial^\mu \theta_H^B \\ & + \Lambda_A^4 \cos(\hat{U}_B^A \lambda_B \theta_H^B) + \Lambda_a^4 \cos\left[p_i^a \hat{n}_b^i \theta_L^b + p_i^a (f^{-2})^{ij} \hat{q}_j^A (f_H^2)_{AB} \theta_H^B \right] \\ & + \frac{1}{32\pi^2} \left[k_{Xi} \hat{n}_a^i \theta_L^a + k_{Xi} (f^{-2})^{ij} \hat{q}_j^A (f_H^2)_{AB} \theta_H^B \right] F_{\mu\nu}^X \tilde{F}^{X\mu\nu} \\ & + \left[c_{\psi i} \hat{n}_a^i \partial_\mu \theta_L^a + c_{\psi i} (f^{-2})^{ij} \hat{q}_j^A (f_H^2)_{AB} \partial_\mu \theta_H^B \right] \bar{\psi} \bar{\sigma}^\mu \psi + \cdots, \end{aligned} \tag{54.}$$

with the block-diagonalized kinetic metric given by

$$(f_L^2)_{ab} = \hat{n}_a^i f_{ij}^2 \hat{n}_b^j, \quad (f_H^2)_{AB} (f_H^{-2})^{BC} = \delta_C^A \ \text{ for } \ (f_H^{-2})^{AB} = \hat{q}_i^A (f^{-2})^{ij} \hat{q}_j^B. \tag{55.}$$

Equation 54 shows that, in the new field basis, mixings between heavy axions θ_H^A and light axions θ_L^a are suppressed by $\Lambda_a^4 / \Lambda_A^4 \ll 1$ and so can be ignored. In contrast, the discrete symmetry (Equation 48) takes a more complicated form as $\mathbb{Z}^N = \mathbb{Z}^{N_L} \times \mathbb{Z}^{N_H}$, with

$$\begin{aligned} & \mathbb{Z}^{N_L} : \ \theta_L^a \to \theta_L^a + 2\pi \ell^a, \\ & \mathbb{Z}^{N_H} : \ \theta_H^A \to \theta_H^A + 2\pi \ell^A, \ \ \theta_L^a \to \theta_L^a - 2\pi \ell^A \hat{q}_i^a (f^{-2})^{ij} \hat{q}_j^B (f_H^2)_{BA}, \end{aligned} \tag{56.}$$

for $\ell^a, \ell^A \in \mathbb{Z}$. Equation 56 implies that, while θ_L^a are 2π periodic by themselves, θ_H^A are 2π periodic *modulo* the shifts of light axions $\Delta\theta_L^a = 2\pi\hat{q}_i^a (f^{-2})^{ij} \hat{q}_j^B (f_H^2)_{BA}$. As a result, for a gauge field strength $F_{\mu\nu}^X$ that couples to light axions θ_L^a, couplings of θ_H^A to $F_{\mu\nu}^X \tilde{F}^{X\mu\nu}$ are generically nonquantized, while couplings of θ_L^a remain to be quantized.

Our major concern is the possibility to generate a hierarchy among the low-energy couplings of the light axions θ_L^a without introducing hierarchical parameters in the underlying UV model. Prior to discussing this issue, we make a small digression to mention the coupling hierarchy of θ_H^A in Reference 38; this coupling hierarchy relies on the hierarchical structure of the original axion scales f_{ij}^2 and thus has characteristics different from those of the coupling hierarchies of θ_L^a that are discussed below. If f_{ij}^2 have hierarchical eigenvalues and $\hat{q}_i^A$ is well aligned with the large eigenvalue direction while having sizable mixing with the small eigenvalue direction, there exists a parameter region with $\langle \theta_H^A | \theta^i \rangle = (f^{-2})^{ij} \hat{q}_j^B (f_H^2)_{BA} \gg 1$ for some i, A. Such parameter values can enhance the coupling of θ_H^A to gauge fields relative to the coupling to generate the leading potential. A simple example is the photophilic QCD axion model discussed in Reference 38; this model involves two axions with

$$f_{ij}^2 = \begin{pmatrix} f_1^2 & \epsilon f_1 f_2 \\ \epsilon f_1 f_2 & f_2^2 \end{pmatrix}, \quad \vec{q}^A = (0,1), \quad \vec{k}_\gamma = (k_1, k_2), \tag{57.}$$

where $f_2 > \epsilon f_2 \gg f_1$, $q_i^A = \hat{q}_i^A$ is the coupling of θ^i to the gluon anomaly generating the QCD axion potential as the last term in Equation 27 and $k_{\gamma i}$ is the coupling to the photon. Then $a(x) = f_H \theta_H^A(x)$ ($\theta_H^A = \theta_2, f_H \simeq f_2$) can be identified as the QCD axion with a decay constant f_H, whose coupling to the photon is enhanced as

$$g_{a\gamma} \simeq \frac{\epsilon f_2}{f_1} \frac{\alpha_{\rm em}}{2\pi} \frac{k_1}{f_H} \gg \frac{\alpha_{\rm em}}{2\pi} g_{a\Lambda} = \frac{\alpha_{\rm em}}{2\pi} \frac{1}{f_H}. \tag{58.}$$

Let us now return to the main issue. To examine the low-energy couplings of θ_L^a, we integrate out the heavy axions θ_H^A. Ignoring the small corrections of $\mathcal{O}(\Lambda_a^4/\Lambda_A^4)$, the vacuum solution of heavy axions is given by $\theta_H^A = 0$ for an arbitrary background of θ_L^a. Upon applying $\theta_H^A = 0$ to Equation 52, the vacuum manifold of V_H is parameterized as

$$\theta^i = \hat{n}_a^i \theta_L^a, \tag{59.}$$

and the effective Lagrangian of the corresponding light axions is given by

$$\begin{aligned} \mathcal{L}_{\rm eff} = & \frac{1}{2} (f_L^2)_{ab} \partial_\mu \theta_L^a \partial^\mu \theta_L^b + \Lambda_a^4 \cos(p_i^a \hat{n}_b^i \theta_L^b) \\ & + \frac{k_{Xi} \hat{n}_a^i \theta_L^a}{32\pi^2} F^X \tilde{F}^X + c_{\psi i} \hat{n}_a^i \partial_\mu \theta_L^a \bar{\psi} \bar{\sigma}^\mu \psi + \cdots . \end{aligned} \tag{60.}$$

This effective Lagrangian suggests that—even when the UV Lagrangian (Equation 46) does not involve any hierarchical parameter, e.g., all dimensionless parameters in Equation 46 are of order unity and all eigenvalues of f_{ij}^2 have a similar size—if $|\hat{n}_a| \gg 1$ can be obtained from $\vec{q}^A$ with $|\vec{q}^A| = \mathcal{O}(1)$, the light axion couplings will have a hierarchical pattern determined by the relative angles between $\hat{n}_a$ and $\{\vec{p}^a, \vec{k}_X, \vec{c}_\psi\}$. Another consequence of $|\hat{n}_a| \gg 1$ is that the light axion decay constants are enlarged as $(f_L)_{ab}^2 = \hat{n}_a^i f_{ij}^2 \hat{n}_b^j \gg f_{ij}^2$.

In fact, $|\hat{n}_a| \gg 1$ is a generic feature of the axion landscape scenario with $N_H \gg N_L$ (33, 145). To see this, we first note that block diagonalization of the axion kinetic terms by Equation 52 leads to the following identity for the field space volume of canonically normalized axions:

$$\det(f_L^2)\det(f_H^2) = \det(f^2). \tag{61.}$$

We also find

$$\det(\hat{n}_a \cdot \hat{n}_b) = \det(\hat{q}^A \cdot \hat{q}^B), \tag{62.}$$

where $\hat{n}_a = (\hat{n}_a^1, \ldots, \hat{n}_a^N)$ and $\hat{q}^A = (\hat{q}_1^A, \ldots, \hat{q}_N^A)$. This relation can be obtained from Equation 61 by taking $f_{ij}^2 = f_0^2\delta_{ij}$ but is valid independently of f_{ij}^2. We can further take an average of this relation over the Gaussian distribution of $\hat{q}_i^A$, and we find (155)

$$\left\langle \det(\hat{n}_a \cdot \hat{n}_b) \right\rangle = \left\langle \det(\hat{q}^A \cdot \hat{q}^B) \right\rangle \sim \left\langle |\hat{q}|^2 \right\rangle^{N_H} \quad (N_H \gg 1), \tag{63.}$$

where $|\hat{q}|^2 = \sum_{A,i}(\hat{q}_i^A)^2/N_H$. Unless $\hat{q}_i^A$ have a highly specific form like $\hat{q}_i^A = \delta_i^A$, we have $|\hat{q}|^2 > 1$. Then, Equation 63 implies that in the limit $N_H \gg N_L$ the generic value of $|\hat{n}_a|$ is exponentially large as

$$|\hat{n}_a| \sim |\hat{q}|^{N_H/N_L}, \tag{64.}$$

where $|\hat{q}|$ (>1) is comparable to the typical value of $|\vec{q}^A|/\mathrm{gcd}(\vec{q}^A)$. With this, the light axion decay constants are exponentially enlarged as $f_L \sim |\hat{q}|^{N_H/N_L} f$, and the effective couplings of θ_L^a can have an exponential hierarchy determined by the relative angles between $\hat{n}_a$ and $\{\vec{p}^a, \vec{k}_X, \vec{c}_\psi\}$. We stress that this is the consequence of the periodic nature of axions, which requires that all components of $\hat{n}_a$ be integer valued. As the light axion directions represent the degenerate vacuum solution of $V_H = -\Lambda_A^4 \cos(q_i^A\theta^i)$, $\hat{n}_a$ should be orthogonal to N_H linearly independent $\vec{q}^A$s. However, when $N_H \gg N_L$, it is exponentially difficult for $\hat{n}_a$ to point in the right direction with only $\mathcal{O}(1)$ integer-valued components, so $|\hat{n}_a|$ are typically forced to have exponentially large values.

Our discussion so far is on the generic feature of the axion landscape scenario, which can be relevant for axion coupling hierarchies. Let us now proceed with explicit examples. For simplicity, we consider the case of single light axion ($N_L = 1$), for which (33)

$$\hat{n}^i \equiv \hat{n}_a^i = \frac{1}{\mathrm{gcd}(\vec{\mathcal{N}})}\mathcal{N}^i, \quad \text{with} \quad \mathcal{N}^i = \det\begin{pmatrix} \delta_1^i & \cdots & \delta_N^i \\ q_1^1 & \cdots & q_N^1 \\ \vdots & \ddots & \vdots \\ q_1^{N_H} & \cdots & q_N^{N_H} \end{pmatrix}. \tag{65.}$$

Our first example is a two-axion model ($N_H = N_L = 1$) realizing the mechanism for enlarging the monotonic field range of the light axion described in References 31 and 156, termed the KNP alignment. The relevant model parameters of our example are given by

$$f_{ij}^2 = f_0^2\delta_{ij}, \quad \vec{q}^A = \vec{q} = (q_1, q_2), \quad \vec{p}^a = \vec{p} = (p_1, p_2), \tag{66.}$$

where $\vec{q}^A$ and $\vec{p}^a$ determine V_H and V_L as in Equation 47. Then the canonically normalized light axion component and its potential are determined as

$$a_L = f_0 \frac{\hat{n}\cdot\vec{\theta}}{|\hat{n}|}, \quad V_L = -\Lambda_a^4 \cos\left(g_{a\Lambda} a_L\right) = -\Lambda_a^4 \cos\left(\frac{\hat{n}\cdot\vec{p}}{|\hat{n}| f_0} a_L\right), \tag{67.}$$

with

$$\hat{n} = \frac{1}{\gcd(q_1, q_2)}(q_2, -q_1). \tag{68.}$$

The monotonic field range of the light axion potential, i.e., $\Delta a_L = 1/g_{a\Lambda} = f_0|\hat{n}|/|\hat{n}\cdot\vec{p}|$, becomes much bigger than the original scale f_0 in the KNP alignment limit where $\vec{q}$ and $\vec{p}$ are aligned to be nearly parallel, giving $0 < |\hat{n}\cdot\vec{p}| \ll |\hat{n}|$. If any of $\vec{q}$ and $\vec{p}$ were a real-valued vector, such an alignment could be made with $|\vec{q}| = \mathcal{O}(1)$. However for periodic axions, both $\vec{q}$ and $\vec{p}$ are integer valued, so $|\hat{n}\cdot\vec{p}| = 0$ or ≥ 1. Accordingly, the KNP alignment requires $|\vec{q}| \geq |\hat{n}| \gg 1$. This outcome implies that the KNP mechanism can yield $\Delta a_L \gg f_0$ and the coupling hierarchies, but at the expense of introducing a large integer-valued input parameter.

The original motivation of the KNP mechanism was to get $\Delta a_L > M_P$, starting from a UV model with $f_0 \ll M_P$ (31). It has been widely discussed that such a trans-Planckian field range obtained by the KNP mechanism may conflict with the axion WGC. In those discussions applied to the model of Equation 66, one often identifies $\vec{g}_{aH} = \vec{q}/f_0$ and $\vec{g}_{aL} = \vec{p}/f_0$ as the axion-instanton couplings spanning the convex hull constrained by the WGC, and we find that the corresponding convex hull cannot satisfy Equation 31 while giving $\Delta a_L = f_0|\hat{n}|/|\hat{n}\cdot\vec{p}| > M_P$ (27–29, 65–67). However, as discussed in Section 2.3, in our viewpoint the axion WGC only implies the existence of certain instanton couplings whose convex hull satisfies Equation 31, but it does not require that the axion potential be determined dominantly by those instanton couplings (26, 29, 30, 65). This fact allows the model (Equation 66) to give rise to $\Delta a_L > M_P$ without any conflict with the axion WGC. Yet the axion WGC indicates that there exists an instanton with coupling $\vec{g}_{\mathcal{I}} = \vec{p}_{\mathcal{I}}/f_0$ not aligned with $\vec{g}_{aH} = \vec{q}/f_0$, which makes a negligible contribution to the axion potential. Then, $\Delta a_L > M_P$ can be obtained through the KNP alignment of $\vec{g}_{aH} = \vec{q}/f_a$ and $\vec{g}_{aL} = \vec{p}/f_a$, while the WGC condition (Equation 31) is fulfilled by the convex hull spanned by $\vec{g}_{aH} = \vec{q}/f_0$ and $\vec{g}_{a\mathcal{I}} = \vec{p}_{\mathcal{I}}/f_0$. In such a case, the two effective couplings of the light axion a_L, i.e., $g_{a\Lambda} = |\hat{n}\cdot\vec{p}|/|\hat{n}|f_0 < 1/M_P$ and $g_{a\mathrm{WGC}} = |\hat{n}\cdot\vec{p}_{\mathcal{I}}|/|\hat{n}|f_0 > S_I/M_P$, have hierarchically different sizes (157, 158).

A potential drawback of the KNP model is that it requires a large integer-valued input parameter to have $|\vec{q}^A| \gg 1$. Our discussion leading to Equation 63 implies that this drawback disappears in models with many axions. Statistical analysis also suggests that the scheme becomes more efficient with a larger number of axions (33, 145). In the case with N ($\gg 1$) axions, the model can be defined on the linear quiver (159) with N sites for the angular axions $\theta^i \cong \theta^i + 2\pi$. One may then assume that axion couplings in the quiver involve only the nearest two sites. Under this assumption, the $N_H = N - 1$ linearly independent couplings to generate the heavy axion potential are given by

$$q_i^A = q_A \delta_i^A - q'_A \delta_{i-1}^A \quad (q_A, q'_A \in \mathbb{Z}). \tag{69.}$$

Among such models, a particularly interesting example is the clockwork axion model (33–35) with

$$f_{ij}^2 = f_0^2 \delta_{ij}, \quad q_A = q, \quad q'_A = 1 \quad \forall\ A. \tag{70.}$$

The clockwork mechanism naturally arranges such that

$$\hat{n} = (1, q, q^2, \ldots, q^{N-1}). \tag{71.}$$

In the quiver description, $\hat{n}_a^i$ can be interpreted as the wave function profile of the light axion along the linear quiver, with which many of the low-energy properties of the light axion can be understood (148).

To examine the effective couplings of the light axion $a_L = f_0 \hat{n} \cdot \vec{\theta}/|\hat{n}|$ in the clockwork axion model, let us introduce the following additional couplings:

$$\vec{g}_{a\Lambda} = \frac{\vec{p}}{f_0}, \quad \vec{g}_{a\mathcal{I}} = \frac{\vec{p}_{\mathcal{I}}}{f_0}, \quad \vec{g}_{aX} = \frac{g_X^2}{8\pi^2}\frac{\vec{k}_X}{f_0}. \tag{72.}$$

Here $\vec{g}_{a\Lambda}$ is coupling to generate the leading potential of the light axion; $\vec{g}_{a\mathcal{I}}$ is coupling to generate an additional but subleading potential, e.g., coupling to the WGC instanton satisfying the bound (Equation 31) or coupling for the barrier potential $V_{\rm br}$ of the relaxion; and $\vec{g}_{aX}$ is coupling to $F^X_{\mu\nu}\tilde{F}^{X\mu\nu}$. One can again assume that integer-valued $\vec{p}, \vec{p}_{\mathcal{I}}$ and $\vec{k}_X$ involve at most the nearest two sites in the quiver. Here we choose the simplest option involving a specific single site, as it gives essentially the same result:

$$p_i = \delta_i^{N_1}, \quad p_{\mathcal{I}i} = \delta_i^{N_2}, \quad k_{Xi} = \delta_i^{N_3}, \tag{73.}$$

where $1 \le N_\ell \le N$ ($\ell = 1, 2, 3$). Then the low-energy effective couplings of the light axion are given by

$$\begin{aligned} g_{a\Lambda} &= \frac{\hat{n}\cdot\vec{g}_{a\Lambda}}{|\hat{n}|} = \frac{q^{N_1-1}}{f_L}, \quad g_{aX} = \frac{g_X^2}{8\pi^2}\frac{\hat{n}\cdot\vec{g}_{aX}}{|\hat{n}|} = \frac{g_X^2}{8\pi^2}\frac{q^{N_3-1}}{f_L}, \\ g_{a\mathcal{I}} &= \frac{\hat{n}\cdot\vec{g}_{a\mathcal{I}}}{|\hat{n}|} = \frac{q^{N_2-1}}{f_L}, \quad (\mathcal{I} = \text{WGC or br}) \end{aligned} \tag{74.}$$

with an exponentially enlarged decay constant

$$f_L = |\hat{n}| f_0 = \sqrt{\frac{q^{2N}-1}{q^2-1}}\, f_0 \sim q^{N-1} f_0. \tag{75.}$$

The above results show that, with appropriately chosen $1 \le N_\ell \le N$, the model can have an exponentially enlarged monotonic field range $\Delta a_L = 1/g_{a\Lambda} \sim q^{N-N_1} f_0$ of the light axion, which can be trans-Planckian while satisfying the WGC bound (Equation 31) with $g_{a\rm WGC} = \mathcal{O}(1/f_0) \gg g_{a\Lambda}$. The model also exhibits a variety of exponential hierarchies among low-energy axion couplings. Additionally, exponentially enlarged $\Delta a_L \propto q^{N-N_1}$ can easily overcome the possible suppression of $f_0 \propto 1/N^p$ ($p = 3$–4) that was observed for some string theory axions in Reference 160. The above clockwork mechanism can be generalized to fields with nonzero spin to generate various parameter hierarchies in particle physics (36). It also has the continuum limit $N \to \infty$, leading to an extradimensional realization of the clockwork mechanism (36, 148, 150). Although interesting, these generalizations are beyond the scope of this review.

4. SUMMARY AND CONCLUSION

Axions have rich physical consequences described by a variety of coupling or scale parameters. Among those parameters are (*a*) coupling $g_{a\Lambda}$ that generates the leading term in the axion potential, which defines the monotonic field range of the potential and the possible cosmological excursion of the axion field; (*b*) couplings to SM particles, particularly couplings to the photon, nucleon, and electron; and (*c*) axion-instanton couplings suggested by the WGC. An interesting feature of the axion parameter space is that there can be hierarchies among the different couplings of a given axion; such hierarchies have good physics motivations and at the same time are technically natural. For instance, the parameter regions that are most accessible by ongoing or planned axion search experiments, including astrophysical and cosmological observations, often correspond to regions where axion couplings have large hierarchies. The hierarchy between $g_{a\Lambda}$ and axion couplings to gauge fields in the SM or the hidden sector has been exploited with a variety of different cosmological or astrophysical motivations. The relaxion idea to solve the weak scale hierarchy problem essentially trades the technically unnatural hierarchy between the weak scale and the cutoff scale for a technically natural but typically bigger hierarchy between $g_{a\Lambda}$ and other relaxion couplings. Given the WGC bound on certain axion-instanton couplings, a trans-Planckian (or nearly Planckian) axion field excursion may imply a hierarchy between $g_{a\Lambda}$ and couplings to the WGC instantons.

In this article, we review recent developments in axion physics while paying particular attention to hierarchies between axion couplings. We first summarize the existing observational constraints on axion couplings, as well as the projected sensitivity limits of planned experiments, which are displayed in **Figures 1** and **2**. For comparison, we also show in **Figures 1** and **2** the parameter ratios that exhibit certain axion coupling hierarchies. It is apparent that the parameter regions of greatest experimental interest require large hierarchies between axion couplings. In the theory of axions, such hierarchies are always technically natural. But it is important to show also that these hierarchies can follow from simple model-building mechanisms. Therefore, after presenting examples of well-motivated axion coupling hierarchies, we discuss model-building attempts to generate hierarchical axion couplings in low-energy effective theory. We focus on a specific scheme that is based on a landscape of many axions, and we show that the required coupling hierarchies appear naturally in this setting. The presence of many axions with very different scales of potentials is common in string theory, so this scheme might be realized in certain areas of the string landscape. The scheme is quite efficient. It can generate an exponential hierarchy among low-energy axion couplings with appropriately chosen $\mathcal{O}(1)$ integer-valued parameters in UV theory. Ideas connected with axion coupling hierarchies mesh attractively with the regions of axion parameter space that will be probed in the near future by ongoing and planned experiments.

DISCLOSURE STATEMENT

The authors are not aware of any affiliations, memberships, funding, or financial holdings that might be perceived as affecting the objectivity of this review.

ACKNOWLEDGMENTS

We thank M.E. Peskin for many valuable comments and suggestions for improving earlier drafts of this article. We also thank D.E. Kaplan, Hyungjin Kim, L.D. Luzio, D.J.E. Marsh, G. Perez, S. Rajendran, G. Servant, G. Shiu, and P. Soler for useful comments and feedback. This work is supported by the Institute for Basic Science under project code IBS-R018-D1.

LITERATURE CITED

1. Kim JE, Carosi G. *Rev. Mod. Phys.* 82:557–602 (2010). Erratum. *Rev. Mod. Phys.* 91:049902 (2019)
2. Marsh DJE. *Phys. Rep.* 643:1–79 (2016)
3. Di Luzio L, Giannotti M, Nardi E, Visinelli L. *Phys. Rep.* 870:1–117 (2020)
4. Svrcek P, Witten E. *J. High Energy Phys.* 06:051 (2006)
5. Arvanitaki A, et al. *Phys. Rev. D* 81:123530 (2010)
6. Peccei RD, Quinn HR. *Phys. Rev. Lett.* 38:1440–43 (1977)
7. Weinberg S. *Phys. Rev. Lett.* 40:223–26 (1978)
8. Wilczek F. *Phys. Rev. Lett.* 40:279–82 (1978)
9. Freese K, Frieman JA, Olinto AV. *Phys. Rev. Lett.* 65:3233–36 (1990)
10. Graham PW, Kaplan DE, Rajendran S. *Phys. Rev. Lett.* 115(22):221801 (2015)
11. Preskill J, Wise MB, Wilczek F. *Phys. Lett. B* 120:127–32 (1983)
12. Abbott LF, Sikivie P. *Phys. Lett. B* 120:133–36 (1983)
13. Dine M, Fischler W. *Phys. Lett. B* 120:137–41 (1983)
14. Arias P, et al. *J. Cosmol. Astropart. Phys.* 06:013 (2012)
15. Meyer M, Horns D, Raue M. *Phys. Rev. D* 87(3):035027 (2013)
16. Córsico AH, et al. *J. Cosmol. Astropart. Phys.* 07:036 (2016)
17. Kohri K, Kodama H. *Phys. Rev. D* 96(5):051701 (2017)
18. Choi K, Im SH. *J. High Energy Phys.* 12:093 (2016)
19. Flacke T, et al. *J. High Energy Phys.* 06:050 (2017)
20. Banerjee A, et al. *J. High Energy Phys.* 07:153 (2020)
21. Graham PW, et al. *Annu. Rev. Nucl. Part. Sci.* 65:485–514 (2015)
22. Irastorza IG, Redondo J. *Prog. Part. Nucl. Phys.* 102:89–159 (2018)
23. Sikivie P. *Rev. Mod. Phys.* 93(1):015004 (2021)
24. Grin D, et al. arXiv:1904.09003 [astro-ph.CO] (2019)
25. Arkani-Hamed N, Motl L, Nicolis A, Vafa C. *J. High Energy Phys.* 06:060 (2007)
26. de la Fuente A, Saraswat P, Sundrum R. *Phys. Rev. Lett.* 114(15):151303 (2015)
27. Rudelius T. *J. Cosmol. Astropart. Phys.* 09:020 (2015)
28. Montero M, Uranga AM, Valenzuela I. *J. High Energy Phys.* 08:032 (2015)
29. Brown J, Cottrell W, Shiu G, Soler P. *J. High Energy Phys.* 10:023 (2015)
30. Saraswat P. *Phys. Rev. D* 95(2):025013 (2017)
31. Kim JE, Nilles HP, Peloso M. *J. Cosmol. Astropart. Phys.* 01:005 (2005)
32. Dimopoulos S, Kachru S, McGreevy J, Wacker JG. *J. Cosmol. Astropart. Phys.* 08:003 (2008)
33. Choi K, Kim H, Yun S. *Phys. Rev. D* 90:023545 (2014)
34. Choi K, Im SH. *J. High Energy Phys.* 01:149 (2016)
35. Kaplan DE, Rattazzi R. *Phys. Rev. D* 93(8):085007 (2016)
36. Giudice GF, McCullough M. *J. High Energy Phys.* 02:036 (2017)
37. Farina M, Pappadopulo D, Rompineve F, Tesi A. *J. High Energy Phys.* 01:095 (2017)
38. Agrawal P, Fan J, Reece M, Wang LT. *J. High Energy Phys.* 02:06 (2018)
39. Kim JE. *Phys. Rev. Lett.* 43:103 (1979)
40. Shifman MA, Vainshtein AI, Zakharov VI. *Nucl. Phys. B* 166:493–506 (1980)
41. Dine M, Fischler W, Srednicki M. *Phys. Lett. B* 104:199–202 (1981)
42. Zhitnitsky AR. *Sov. J. Nucl. Phys.* 31:260 (1980)
43. Witten E. *Phys. Lett. B* 149:351–56 (1984)
44. Choi K. *Phys. Rev. D* 62:043509 (2000)
45. Banks T, Dine M, Fox PJ, Gorbatov E. *J. Cosmol. Astropart. Phys.* 06:001 (2003)
46. Choi K, Kim JE. *Phys. Lett. B* 154:393 (1985). Erratum. *Phys. Lett. B* 156:452 (1985)
47. Akrami Y, et al. *Astron. Astrophys.* 641:A10 (2020)
48. Borsanyi S, et al. *Nature* 539(7627):69–71 (2016)
49. Hui L, Ostriker JP, Tremaine S, Witten E. *Phys. Rev. D* 95(4):043541 (2017)
50. Georgi H, Kaplan DB, Randall L. *Phys. Lett. B* 169:73–78 (1986)
51. Silverstein E, Westphal A. *Phys. Rev. D* 78:106003 (2008)

52. Srednicki M. *Nucl. Phys. B* 260:689–700 (1985)
53. Chang S, Choi K. *Phys. Lett. B* 316:51–56 (1993)
54. Kaplan DB. *Nucl. Phys. B* 260:215–26 (1985)
55. Leutwyler H, Shifman MA. *Phys. Lett. B* 221:384–88 (1989)
56. Chivukula RS, Cohen AG, Georgi H, Manohar AV. *Phys. Lett. B* 222:258–62 (1989)
57. Grilli di Cortona G, Hardy E, Pardo Vega J, Villadoro G. *J. High Energy Phys.* 01:034 (2016)
58. Borsanyi SZ, et al. arXiv:2007.03319 [hep-lat] (2020)
59. Moody JE, Wilczek F. *Phys. Rev. D* 30:130 (1984)
60. Bertolini S, Di Luzio L, Nesti F. *Phys. Rev. Lett.* 126(8):081801 (2021)
61. Gunion JF, Gamberini G, Novaes SF. *Phys. Rev. D* 38:3481 (1988)
62. Palti E. *Fortsch. Phys.* 67(6):1900037 (2019)
63. Cheung C, Remmen GN. *Phys. Rev. Lett.* 113:051601 (2014)
64. Dine M, Seiberg N, Wen XG, Witten E. *Nucl. Phys. B* 278:769–89 (1986)
65. Brown J, Cottrell W, Shiu G, Soler P. *J. High Energy Phys.* 04:017 (2016)
66. Heidenreich B, Reece M, Rudelius T. *J. High Energy Phys.* 12:108 (2015)
67. Hebecker A, Mangat P, Theisen S, Witkowski LT. *J. High Energy Phys.* 02:097 (2017)
68. Blumenhagen R, Cvetic M, Kachru S, Weigand T. *Annu. Rev. Nucl. Part. Sci.* 59:269–96 (2009)
69. Sikivie P. *Phys. Rev. Lett.* 51:1415–17 (1983). Erratum. *Phys. Rev. Lett.* 52:695 (1984)
70. Khatiwada R, et al. arXiv:2010.00169 [astro-ph.IM] (2020)
71. Semertzidis YK, et al. arXiv:1910.11591 [physics.ins-det] (2019)
72. Beurthey S, et al. arXiv:2003.10894 [physics.ins-det] (2020)
73. Kahn Y, Safdi BR, Thaler J. *Phys. Rev. Lett.* 117(14):141801 (2016)
74. Obata I, Fujita T, Michimura Y. *Phys. Rev. Lett.* 121(16):161301 (2018)
75. Marsh DJE, et al. *Phys. Rev. Lett.* 123(12):121601 (2019)
76. Berlin A, D'Agnolo RT, Ellis SAR, Zhou K. arXiv:2007.15656 [hep-ph] (2020)
77. Zyla PA, et al. (Part. Data Group). *Prog. Theor. Exp. Phys.* 2020(8):083C01 (2020)
78. Cadamuro D, Redondo J. *J. Cosmol. Astropart. Phys.* 02:032 (2012)
79. Bähre R, et al. *J. Instrum.* 8:T09001 (2013)
80. Vinyoles N, et al. *J. Cosmol. Astropart. Phys.* 10:015 (2015)
81. Armengaud E, et al. *J. Cosmol. Astropart. Phys.* 06:047 (2019)
82. Reynolds CS, et al. *Astrophys. J.* 890:59 (2020)
83. Gramolin AV, et al. *Nat. Phys.* 17:79–84 (2021)
84. Henning R, et al. (ABRACADABRA Collab.). DESY-PROC-2017-02 (2018)
85. Jackson Kimball DF, et al. *Springer Proc. Phys.* 245:105–21 (2020)
86. Graham PW, et al. *Phys. Rev. D* 97(5):055006 (2018)
87. Bloch IM, Hochberg Y, Kuflik E, Volansky T. *J. High Energy Phys.* 01:167 (2020)
88. Graham PW, et al. *Phys. Rev. D* 103:055010 (2021)
89. Crescini N, et al. *Phys. Rev. Lett.* 124(17):171801 (2020)
90. Acciarri M, et al. (L3 Collab.). *Phys. Lett. B* 385:454–70 (1996)
91. Schael S, et al. (LEP Work. Group Higgs Boson Searches). *Eur. Phys. J. C* 47:547–87 (2006)
92. O'Hare CAJ, Vitagliano E. *Phys. Rev. D* 102:115026 (2020)
93. Hardy E, Lasenby R. *J. High Energy Phys.* 02:033 (2017)
94. Benato G, Drobizhev A, Rajendran S, Ramani H. *Phys. Rev. D* 99(3):035025 (2019)
95. Graham PW, et al. *Phys. Rev. D* 93(7):075029 (2016)
96. Badurina L, et al. *J. Cosmol. Astropart. Phys.* 05:011 (2020)
97. El-Neaj YA, et al. *EPJ Quant. Technol.* 7:6 (2020)
98. Feng JL, Galon I, Kling F, Trojanowski S. *Phys. Rev. D* 97(5):055034 (2018)
99. Arvanitaki A, Geraci AA. *Phys. Rev. Lett.* 113(16):161801 (2014)
100. Geraci AA, et al. *Springer Proc. Phys.* 211:151–61 (2018)
101. Hlozek R, Grin D, Marsh DJE, Ferreira PG. *Phys. Rev. D* 91(10):103512 (2015)
102. Hlozek R, Marsh DJE, Grin D. *Mon. Not. R. Astron. Soc.* 476(3):3063–85 (2018)
103. Poulin V, et al. *Phys. Rev. D* 98(8):083525 (2018)

104. Bauer JB, et al. *Mon. Not. R. Astron. Soc.* 500(3):3162–77 (2020)
105. Porayko NK, et al. *Phys. Rev. D* 98(10):102002 (2018)
106. Kobayashi T, et al. *Phys. Rev. D* 96(12):123514 (2017)
107. Aghamousa A, et al. arXiv:1611.00036 [astro-ph.IM] (2016)
108. Marsh DJE, Niemeyer JC. *Phys. Rev. Lett.* 123(5):051103 (2019)
109. Hu W, Barkana R, Gruzinov A. *Phys. Rev. Lett.* 85:1158–61 (2000)
110. Seljak U, Zaldarriaga M. *Phys. Rev. Lett.* 82:2636–39 (1999)
111. Arvanitaki A, Dubovsky S. *Phys. Rev. D* 83:044026 (2011)
112. Brito R, Cardoso V, Pani P. *Lect. Notes Phys.* 906:1–237 (2015)
113. Gruzinov A. arXiv:1604.06422 [astro-ph.HE] (2016)
114. Baryakhtar M, Galanis M, Lasenby R, Simon O. arXiv:2011.11646 [hep-ph] (2020)
115. Arvanitaki A, Baryakhtar M, Huang X. *Phys. Rev. D* 91(8):084011 (2015)
116. Stott MJ. arXiv:2009.07206 [hep-ph] (2020)
117. Fukuda H, Nakayama K. *J. High Energy Phys.* 01:128 (2020)
118. Mathur A, Rajendran S, Tanin EH. *Phys. Rev. D* 102(5):055015 (2020)
119. Higaki T, Jeong KS, Kitajima N, Takahashi F. *Phys. Lett. B* 755:13–16 (2016)
120. Dror JA, Leedom JM. *Phys. Rev. D* 102(11):115030 (2020)
121. Darmé L, Di Luzio L, Giannotti M, Nardi E. *Phys. Rev. D* 103(1):015034 (2021)
122. Marques-Tavares G, Teo M. *J. High Energy Phys.* 05:180 (2018)
123. Han C, et al. *Phys. Rev. D* 103(3):035028 (2021)
124. Hardy E. *J. High Energy Phys.* 11:077 (2015)
125. Hook A, Marques-Tavares G. *J. High Energy Phys.* 12:101 (2016)
126. Fonseca N, Morgante E, Servant G. *J. High Energy Phys.* 10:020 (2018)
127. Wang SJ. *Phys. Rev. D* 99(9):095026 (2019)
128. Ibe M, Shoji Y, Suzuki M. *J. High Energy Phys.* 11:140 (2019)
129. Kadota K, Min U, Son M, Ye F. *J. High Energy Phys.* 02:135 (2020)
130. Fonseca N, Morgante E, Sato R, Servant G. *J. High Energy Phys.* 05:080 (2020). Erratum. *J. High Energy Phys.* 01:012 (2021)
131. Hebecker A, Mikhail T, Soler P. *Front. Astron. Space Sci.* 5:35 (2018)
132. Turner MS, Widrow LM. *Phys. Rev. D* 37:2743 (1988)
133. Garretson WD, Field GB, Carroll SM. *Phys. Rev. D* 46:5346–51 (1992)
134. Choi K, Kim H, Sekiguchi T. *Phys. Rev. Lett.* 121(3):031102 (2018)
135. Anber MM, Sorbo L. *Phys. Rev. D* 81:043534 (2010)
136. Notari A, Tywoniuk K. *J. Cosmol. Astropart. Phys.* 12:038 (2016)
137. Adshead P, Wyman M. *Phys. Rev. Lett.* 108:261302 (2012)
138. Agrawal P, Fan J, Reece M. *J. High Energy Phys.* 10:193 (2018)
139. Agrawal P, Marques-Tavares G, Xue W. *J. High Energy Phys.* 03:049 (2018)
140. Kitajima N, Sekiguchi T, Takahashi F. *Phys. Lett. B* 781:684–87 (2018)
141. Agrawal P, et al. *Phys. Lett. B* 801:135136 (2020)
142. Co RT, Pierce A, Zhang Z, Zhao Y. *Phys. Rev. D* 99(7):075002 (2019)
143. Choi K, Seong H, Yun S. *Phys. Rev. D* 102(7):075024 (2020)
144. Amin MA, Mou Z-G. *J. Cosmol. Astropart. Phys.* 02:024 (2021)
145. Higaki T, Takahashi F. *J. High Energy Phys.* 07:074 (2014)
146. Bachlechner TC, Dias M, Frazer J, McAllister L. *Phys. Rev. D* 91(2):023520 (2015)
147. Junghans D. *J. High Energy Phys.* 02:128 (2016)
148. Craig N, Garcia Garcia I, Sutherland D. *J. High Energy Phys.* 10:018 (2017)
149. Bachlechner TC, Eckerle K, Janssen O, Kleban M. *J. High Energy Phys.* 11:036 (2017)
150. Choi K, Im SH, Shin CS. *J. High Energy Phys.* 07:113 (2018)
151. Barr SM, Seckel D. *Phys. Rev. D* 46:539–49 (1992)
152. Kamionkowski M, March-Russell J. *Phys. Lett. B* 282:137–41 (1992)
153. Holman R, et al. *Phys. Lett. B* 282:132–36 (1992)
154. Smith HJS. *Philos. Trans. R. Soc.* 151(1):293–326 (1861)

155. Goodman NR. *Ann. Math. Stat.* 34(1):178–80 (1963)
156. Kappl R, Krippendorf S, Nilles HP. *Phys. Lett. B* 737:124–28 (2014)
157. Kappl R, Nilles HP, Winkler MW. *Phys. Lett. B* 753:653–59 (2016)
158. Choi K, Kim H. *Phys. Lett. B* 759:520–27 (2016)
159. Arkani-Hamed N, Cohen AG, Georgi H. *Phys. Rev. Lett.* 86:4757–61 (2001)
160. Demirtas M, Long C, McAllister L, Stillman M. *J. High Energy Phys.* 04:138 (2020)

Annual Review of Nuclear and Particle Science

Volume 71, 2021

Contents

Errata

An online log of corrections to *Annual Review of Nuclear and Particle Science* articles may be found at http://www.annualreviews.org/errata/nucl